Mass and width of the $\sigma(750)$ scalar meson from measurements of $\pi N \to \pi^- \pi^+ N$ on polarized targets

M. Svec*
Department of Physics, Dawson College, Montreal, Quebec, Canada H3Z 1A4
and McGill University, Montreal, Quebec, Canada H3A 2T8
(Received 18 July 1996; revised manuscript received 23 December 1996)

The measurements of reactions $\pi^- p_\uparrow \to \pi^- \pi^+ n$ at 17.2 GeV/c and $\pi^+ n_\uparrow \to \pi^+ \pi^- p$ at 5.98 and 11.85 GeV/c on polarized targets at CERN provide model-independent and solution-independent evidence for a narrow scalar state $\sigma(750)$. The original χ^2 minimization method and the recent Monte Carlo method for the amplitude analysis of data at 17.2 GeV/c are in excellent agreement. Both methods find that the mass distribution of the measured amplitude $|S|^2\Sigma$ with recoil transversity ''up'' resonates near 750 MeV while the amplitude $|S|^2\Sigma$ with recoil transversity ''down'' is large and nonresonating. The amplitude $|S|^2\Sigma$ contributes as a strong background to S-wave intensity $I_S=(|S|^2+|\overline{S}|^2)\Sigma$ and distorts the determinations of σ resonance parameters from I_S. To avoid this problem we perform a series of Breit-Wigner fits directly to the measured distribution $|\overline{S}|^2\Sigma$. The inclusion of various backgrounds causes the width of $\sigma(750)$ to become very narrow. Our best fit with a t-averaged coherent background yields $m_\sigma=753\pm19$ MeV and $\Gamma_\sigma=108\pm53$ MeV. These values are in excellent agreement with the Ellis-Lanik theorem for the width of scalar gluonium. The gluonium interpretation of $\sigma(750)$ is also supported by the absence of $\sigma(750)$ in reactions $\gamma\gamma\to\pi\pi$. We also show how data on polarized target invalidate essential assumptions of past determinations of $\pi\pi$ phase shifts which explains the absence of $\sigma(750)$ in the conventional phase shift δ_0^0. We examine the interference of $\sigma(750)$ with $f_0(980)$ and find it has only a very small effect on the determination of the $\sigma(750)$ mass and width. The data on the amplitude $|\overline{S}|^2\Sigma$ in the mass range of 1120–1520 MeV show the existence of a scalar resonance $f_0(1300)$ with a mass of 1280 ± 12 MeV and a width of 192 ± 26 MeV. Our results emphasize the need for a systematic study of production processes on the level of spin amplitudes measured in experiments with polarized targets. [S0556-2821(97)05409-X]

PACS number(s): 14.40.Cs, 13.85.Hd, 13.88.+e

I. INTRODUCTION

Amplitude analyses of pion production reactions such as $\pi N \to \pi\pi N$ or $KN \to K\pi N$ are important for two special reasons. First, these reactions provide information about unnatural exchange amplitudes which are not accessible in two-body reactions. Second, such amplitude analyses enable us to study resonance production on the level of spin-dependent amplitudes rather than spin-averaged cross section $d^2\sigma/dmdt$. In 1978, Lutz and Rybicki showed [1] that measurements of pion production in meson-nucleon scattering on transversely polarized target yield in a single experiment enough observables that almost complete and model-independent amplitude analysis can be performed.

The high statistics measurement of $\pi^- p \to \pi^- \pi^+ n$ at 17.2 GeV/c at CERN Proton Synchrotron (PS) on an unpolarized target [2] was later repeated with a transversely polarized proton target at the same energy [3–7]. Model-independent amplitude analyses were performed for various intervals [3–6] of dimeson mass of small momentum transfers $-t=0.005-0.2$ $(\mathrm{GeV}/c)^2$ and over a large interval [7] of momentum transfer $-t=0.2-1.0$ $(\mathrm{GeV}/c)^2$.

Additional information was provided by the first measurement of $\pi^+ n \to \pi^+ \pi^- p$ and $K^+ n \to K^+ \pi^- p$ reactions [8,9] on polarized deuteron target at 5.98 and 11.85 GeV/c, also done at CERN-PS. The data allowed to study the t evolution of the mass dependence of the moduli of amplitudes [10]. Detailed amplitude analyses [11,12] determined the mass dependence of amplitudes at larger momentum transfers $-t=0.2-0.4$ $(\mathrm{GeV}/c)^2$.

All amplitude analyses [3–12] of pion production on polarized targets found clear evidence for large and nontrivial unnatural A_1-exchange amplitudes in the dipion mass range from 400 to 1800 MeV. This experimental finding is very important since previously the A_1 exchange amplitudes were assumed absent. In particular, all determinations of $\pi\pi$ phase shifts from unpolarized data on $\pi^- p \to \pi^- \pi^+ n$ are based on the assumption of vanishing A_1 exchange amplitudes [13–19]. Without this assumption the determination of $\pi\pi$ phase shifts cannot even proceed. The existence of large and nontrivial A_1 exchange amplitudes in $\pi N \to \pi^+ \pi^- N$ reactions casts a serious doubt about the validity of the conventional $\pi\pi$ phase shifts. The existence of A_1 exchange is also crucial for our understanding of the spin structure of the nucleon. All analyses of nucleon internal spin structure depend on the behavior of polarized structure function $g_1(x,Q^2)$ which is controlled by A_1 exchange for $x\to0$ [see Eq. (4.2.23) of Ref. [20]].

Another important finding of measurements of $\pi^- p \to \pi^- \pi^+ n$ and $\pi^+ n \to \pi^+ \pi^- p$ reactions on polarized targets is the evidence for a narrow scalar state $I=0\ 0^{++}(750)$. It is important to recognize that the discovery of this state was possible only because the measurements

*Electronic address: svec@hep.physics.mcgill.ca

on polarized targets enable a model independent separation of the S-wave and P-wave contributions to the reaction cross section $\Sigma \equiv d^2\sigma/dmdt$. Specifically, the data on polarized targets determine the moduli $|S|^2\Sigma$ and $|\overline{S}|^2\Sigma$ of the two S-wave amplitudes with recoil nucleon spin ''down'' and ''up,'' respectively. There are two solutions for $|S|^2\Sigma$, and independently two solutions for $|\overline{S}|^2\Sigma$. Hence, there are four independent solutions for the S-wave intensity $I_S=(|S|^2+|\overline{S}|^2)\Sigma$ which we label $I_S(i,j)$, $i,j=1,2$ with the indices i and j referring to the two solutions for $|S|^2\Sigma$ and $|\overline{S}|^2\Sigma$, respectively.

Motivated by the emerging evidence for the scalar resonance $\sigma(750)$ from several previous analyses [21–24], a new amplitude analysis of measurements of $\pi^-p\to\pi^-\pi^+n$ and $\pi^+n\to\pi^+\pi^-p$ on polarized targets was recently performed [25]. To ascertain the existence of the $\sigma(750)$ state, special attention was paid to error propagation and selection of physical solutions for amplitudes. A clear and solution-independent signal for a narrow $\sigma(750)$ was obtained in this improved analysis. The CERN-Munich data at 17.2 GeV/c and small momentum transfers [4] show resonant behavior at 750 MeV in both solutions for $|S|^2\Sigma$. The Saclay data at 5.98 and 11.85 GeV/c and larger momentum transfers [8] show resonant behavior at 750 MeV in all four solutions for S-wave intensity at both energies. However, only a tentative determination of the mass and width of the $\sigma(750)$ state was attempted in this study.

The aim of the present work is a more reliable determination of mass and width of the $\sigma(750)$ resonance from model-independent amplitude analyses of CERN-Munich data on $\pi^-p\to\pi^-\pi^+n$ on polarized target at 17.2 GeV/c. There are three important issues that we address in the process.

The first issue is the question of which mass distribution should be used for Breit-Wigner fits to determine the resonance parameters of $\sigma(750)$ state. The previous CERN-Munich analyses [5–7] fitted a Breit-Wigner formula to partial wave intensities, and we followed the same procedure in Ref. [25]. However, the S-wave intensity at lower momentum transfers at 17.2 GeV/c shows a clear resonant structure only in solutions $I_S(1,1)$ and $I_S(2,1)$ while the solutions $I_S(1,2)$ and $I_S(2,2)$ lack sufficient decreases of I_S above 800 MeV to indicate a narrow resonance. This behavior in $I_S=(|S|^2+|\overline{S}|^2)\Sigma$ is caused by the large and nonresonating amplitude $|\overline{S}|^2\Sigma$. The amplitude $|\overline{S}|^2\Sigma$ thus behaves as a large and nonresonating background to the resonating amplitude $|S|^2\Sigma$ and this distorts the determination of resonance parameters of $\sigma(750)$ from Breit-Wigner fits to I_S. To avoid this problem, it is necessary to perform Breit-Wigner fits directly to the resonant mass distributions $|S|^2\Sigma$. Both solutions for $|S|^2\Sigma$ resonate and the evidence for $\sigma(750)$ is thus entirely solution independent.

The second issue is which resonance shape formula is to be used in Breit-Wigner fits to $|S|^2\Sigma$. The previous analyses [2,5–7,25] used the Pišút-Roos shape formula which multiplies the standard Breit-Wigner formula (with a phase space) by an additional mass-dependent factor $F=(2J+1)(m/q)^2$. In their analysis of $\pi N\to\pi\pi N$ reaction amplitudes [26], Pišút and Roos assumed the absence of A_1 exchange amplitudes and assumed that the mass dependence of pion production amplitudes is given by $\pi\pi$ scattering amplitudes. The partial wave expansion of $\pi\pi$ amplitudes then directly leads to the additional factor F. However, because of the existence of large and nontrivial A_1 exchange amplitudes in $\pi N\to\pi^+\pi^-N$ reactions and because there is no proof that the mass dependence of $\pi N\to\pi\pi N$ production amplitudes is really described by the energy dependence of partial waves in $\pi\pi$ scattering, it is useful to perform Breit-Wigner fits to the $|S|^2\Sigma$ mass distribution using the standard [27] phenomenological shape formula in which the Pišút-Roos factor is absent (i.e., $F=1$) to see if there are differences in the determination of resonance parameters of $\sigma(750)$. The comparison of fits using both shape formulas finds only small differences.

The third issue is the question of background in the resonant mass distribution $|S|^2\Sigma$. Nonresonating background comes, e.g., from the isospin $I=2$ contribution to $|S|^2\Sigma$. While it is difficult to exactly parametrize the unknown background, we estimated the background contribution using three different approaches. In each case we find that inclusion of background leads to a significant reduction of the width of $\sigma(750)$ to somewhere around 100 MeV. Background is obviously important for the width determination of $\sigma(750)$ and thus to our understanding of the constituent structure of the $\sigma(750)$ state. We also examine the interference of $\sigma(750)$ with $f_0(980)$ and find it has only a small effect on the mass and width of $\sigma(750)$.

The paper is organized as follows. In Sec. II we review the basic formalism and two methods of amplitude analysis. In Sec. III we derive the Pišút-Roos shape formula and describe the phenomenological shape formula for Breit-Wigner fits. In Sec. IV we present our fits to the measured resonating amplitude $|S|^2\Sigma$ and describe our approaches to the inclusion of a coherent background. In Sec. V we study the interference of $\sigma(750)$ with $f_0(750)$ and also perform fits in the broad mass range 600–1520 MeV which show evidence for a scalar resonance $f_0(1300)$. In Sec. VI we present our fits to S-wave intensity I_S in $\pi^-p\to\pi^-\pi^+n$ at 17.2 GeV/c and in $\pi^+n\to\pi^+\pi^-p$ at 5.98 and 11.85 GeV/c. In Sec. VII we review the assumptions of past determinations of $\pi\pi$ phase shifts and show how they are invalidated by the data on polarized targets. This explains the absence of the narrow $\sigma(750)$ state in conventional phase shift δ_0^0. In Sec. VIII we answer critical questions concerning the evidence for a narrow $\sigma(750)$. In Sec. IX we propose to identify the $\sigma(750)$ state with lowest mass gluonium $0^{++}(gg)$ and discuss theoretical and experimental support for this interpretation of $\sigma(750)$. The paper closes with a summary in Sec. X.

II. BASIC FORMALISM

A. Phase space and amplitudes

From the point of view of Breit-Wigner fits to various mass distributions in $\pi^-p\to\pi^-\pi^+n$ it is necessary to determine the part of the phase space which depends on the dipion mass m and contributes to the mass distribution. Consider reaction $a+b\to1+2+3$ such as $\pi^-p\to\pi^-\pi^+n$ with four-momentum conservation $P=p_a+p_b=p_1+p_2+p_3$

$=p_d+p_3$, where $p_d=p_1+p_2$ is the dipion momentum. The spin averaged cross section is given by

$$d\sigma=\frac{1}{\mathrm{Flux}(s)}\frac{1}{(2s_a+1)(2s_b+1)}\sum_{\lambda_n,\lambda_p}|M_{\lambda_n,0\lambda_p}|^2 dX_{\mathrm{LIPS}_3}, \tag{2.1}$$

where the flux

$$\mathrm{Flux}(s)=4\sqrt{(p_a p_b)^2-m_a^2 m_b^2}=4Mp_{\pi\mathrm{lab}} \tag{2.2}$$

with $m_a=\mu$ mass of pion and $m_b=M$ mass of proton. The λ_p and λ_n are the proton and neutron helicities. We will work with the usual kinematic variables of c.m. energy squared s, momentum transfer t, dipion mass m, and angles θ,ϕ describing the angular distribution of π^- in the $\pi^-\pi^+$ rest frame. Following the procedure described on pp. 18 and 19 of Ref. [28] and using $dm^2=2mdm$, we can write the Lorentz-invariant phase space as

$$dX_{\mathrm{LIPS}_3}(P,p_1,p_2,p_3)=q(m^2)G(s)dmdtd\Omega, \tag{2.3}$$

where q is the pion momentum in the c.m. system (c.m.s.) of the dipion system,

$$q(m^2)=\sqrt{0.25m^2-\mu^2}=\frac{m}{2}\sqrt{1-\left(\frac{2\mu}{m}\right)^2} \tag{2.4}$$

and $G(s)$ is the energy-dependent part of phase space:

$$G(s)=\frac{1}{(2\pi)^4}\frac{1}{8\sqrt{[s-(\mu+M)^2][s-(\mu-M)^2]}}. \tag{2.5}$$

Hence

$$\frac{d\sigma}{dmdtd\Omega}=\frac{K(s)}{4\pi}\,q\sum_{\lambda_p,\lambda_n}|M_{\lambda_n,0\lambda_p}(s,t,m,\theta,\phi)|^2, \tag{2.6}$$

where

$$K(s)=\frac{2\pi G(s)}{\mathrm{Flux}(s)}. \tag{2.7}$$

The dipion state does not have a definite spin and helicity. To obtain dipion states of definite spin J and helicity λ, we expand

$$M_{\lambda_n,0\lambda_p}=\sum_{J=0}^{\infty}\sum_{\lambda=-J}^{+J}\sqrt{(2J+1)}M^J_{\lambda\lambda_n,0\lambda_p}(s,t,m)d^J_{\lambda 0}(\theta)e^{i\lambda\phi}. \tag{2.8}$$

We now integrate $|M_{\lambda_n,0\lambda_p}|^2$ over $d\Omega$. Using orthogonality relations for the d functions and spherical harmonics, we obtain, for the reaction cross section,

$$\frac{d^2\sigma}{dmdt}=q(m^2)K(s)\sum_{J=0}^{\infty}\sum_{\lambda,\lambda_n,\lambda_p}|M^J_{\lambda\lambda_n,0\lambda_p}(s,t,m)|^2. \tag{2.9}$$

In Eq. (2.9) it is the amplitudes $M^J_{\lambda\lambda_n,0\lambda_p}$ or their combinations which exhibit a resonant Breit-Wigner behavior. From (2.9) we see that this behavior is modified by a phase space factor $q(m^2)$ which is common to all mass distributions in $\pi N\to\pi^+\pi^-N$.

To introduce the amplitudes required for the amplitude analysis we first define

$$H^J_{\lambda\lambda_n,0\lambda_p}=\sqrt{q(m^2)}\sqrt{K(s)}M^J_{\lambda\lambda_n,0\lambda_p}. \tag{2.10}$$

We will also consider only the $J=0$ (S-wave) and $J=1$ (P-wave) contributions for dipion masses m below 1000 MeV. With a notation

$$\Sigma=d^2\sigma/dmdt, \tag{2.11}$$

we now define normalized helicity amplitudes with a definite t-channel naturality

$$H^0_{0+,0+}=S_0\sqrt{\Sigma},\quad H^0_{0+,0-}=S_1\sqrt{\Sigma},$$
$$H^1_{0+,0+}=L_0\sqrt{\Sigma},\quad H^1_{0+,0-}=L_1\sqrt{\Sigma},$$
$$H^1_{\pm 1+,0+}=\frac{1}{\sqrt{2}}(N_0\pm U_0)\sqrt{\Sigma},$$
$$H^1_{\pm 1+,0-}=\frac{1}{\sqrt{2}}(N_1\pm U_1)\sqrt{\Sigma}. \tag{2.12}$$

In Eq. (2.12) $n=|\lambda_p-\lambda_n|=0,1$ is the nucleon helicity flip. At large s, the unnatural helicity nonflip amplitudes S_0,L_0,U_0 and the unnatural helicity flip amplitudes S_1,L_1,U_1 exchange A_1 and π quantum numbers in the t channel, respectively. Both natural exchange amplitudes N_0 and N_1 exchange A_2 at large s.

The amplitude analysis of data on polarized targets is performed using normalized recoil nucleon transversity amplitudes defined as

$$S=\frac{1}{\sqrt{2}}(S_0+iS_1),\quad \overline{S}=\frac{1}{\sqrt{2}}(S_0-iS_1),$$
$$L=\frac{1}{\sqrt{2}}(L_0+iL_1),\quad \overline{L}=\frac{1}{\sqrt{2}}(L_0-iL_1),$$
$$U=\frac{1}{\sqrt{2}}(U_0+iU_1),\quad \overline{U}=\frac{1}{\sqrt{2}}(U_0-iU_1),$$
$$N=\frac{1}{\sqrt{2}}(N_0-iN_1),\quad \overline{N}=\frac{1}{\sqrt{2}}(N_0+iN_1). \tag{2.13}$$

The amplitudes S,L,U,N and $\overline{S,L,U,N}$ correspond to recoil nucleon transversity ''down'' and ''up,'' respectively [9,11]. The ''up'' direction is the direction of normal to the scattering plane defined according to Basel convention by $\vec{p}_\pi\times\vec{p}_{\pi\pi}$, where $\vec{p}_\pi$ and $\vec{p}_{\pi\pi}$ are the incident pion and dimeson momenta in the target nucleon rest frame.

The normalized transversity amplitudes satisfy condition

$$|S|^2+|\overline{S}|^2+|L|^2+|\overline{L}|^2+|U|^2+|\overline{U}|^2+|N|^2+|\overline{N}|^2=1. \tag{2.14}$$

The unnormalized transversity amplitudes are $|A|^2\Sigma$ and $|\overline{A}|^2\Sigma$, where $A=S,L,U,N$. Finally we define spin-averaged partial wave intensities for amplitudes $A=S,L,U,N$:

$$I_A=(|A_0|^2+|A_1|^2)\Sigma=(|A|^2+|\overline{A}|^2)\Sigma. \tag{2.15}$$

Obviously

$$\Sigma=\frac{d^2\sigma}{dmdt}=I_S+I_L+I_U+I_N. \tag{2.16}$$

B. Two methods of amplitude analysis

For invariant masses below 1000 MeV, the dipion system in reactions $\pi N\to\pi^+\pi^-N$ is produced predominantly in spin states $J=0$ (S wave) and $J=1$ (P wave). The experiments on transversely polarized targets then yield 15 spin-density-matrix (SDM) elements describing the dipion angular distribution [8,9]. The measured SDM elements are expressed in terms of two S-wave and six P-wave normalized transversity amplitudes [Eq. (2.13)] [1,11]. These relations involve eight moduli and six cosines of relative phases of nucleon transversity amplitudes [Eq. (2.13)]. Amplitude analysis expresses analytically [1,11] the eight normalized moduli and the six cosines of relative phases of nucleon transversity amplitudes in terms of measured SDM elements. There are two similar solutions in each (m,t) bin. However, in many (m,t) bins the solutions are unphysical: either a cosine has magnitude larger than one or the two solutions for moduli are complex conjugate with a small imaginary part. Unphysical solutions also complicate the error analysis.

The occurrence of unphysical solutions is a common difficulty in all amplitude analyses. Two methods are used to find physical solutions and determine their errors. They are (a) the χ^2 minimization method and (b) the Monte Carlo method.

In the χ^2 method one minimizes a function

$$\chi^2=\sum_{i=1}^{M}\left[\frac{\mathrm{Obs}_i(\mathrm{meas})-\mathrm{Obs}_i(\mathrm{calc})}{\Delta_i}\right]^2, \tag{2.17}$$

where Obs_i (meas) are the experimentally measured quantities, Δ_i are their experimental errors, and Obs_i (calc) are corresponding expressions in terms of the amplitudes (moduli and cosines of relative phases). The analytical solutions for the moduli and cosines serve as initial values. This χ^2 method was used in all CERN-Munich analyses [3–7] of $\pi^-p\to\pi^-\pi^+p$ at 17.2 GeV/c. Since the two analytical solutions (initial values) are very close, the χ^2 method leads to a unique solution in many (m,t) bins. A particular exception is the mass range below 900 MeV. More recently the χ^2 method was used in direct reconstruction of amplitudes of pp elastic amplitudes from 0.8 to 2.7 GeV using polarized data obtained at SATURN II at Saclay [29].

The basic idea of Monte Carlo method is to vary randomly the input SDM elements within their experimental errors and perform amplitude analysis for each new set of the input SDM elements. The resulting moduli and cosines of relative angles are retained only when all of them have physical values in both analytical solutions. Unphysical solutions are rejected. The distributions of accepted moduli and cosines define the range of their physical values and their average value in each (m,t) bin. The Monte Carlo amplitude analysis of Ref. [25] is based on 30 000 random variations of the input SDM elements. The Monte Carlo method was first used in 1977 in an amplitude analysis [30] of pp elastic scattering at 6 GeV/c and later in an amplitude analysis [31] of reactions $\pi^-p\to K^+K^-n$ and $\pi^-p\to K_S^0K_S^0n$ at 63 GeV/c. In his review paper [32], James advocates the use of the Monte Carlo method as perhaps the only way to calculate the errors in the case of nonlinear functions which produce non-Gaussian distributions. The method has the added advantage that it can separate the physical and unphysical solutions and that it can retain the identity of the two analytical solutions.

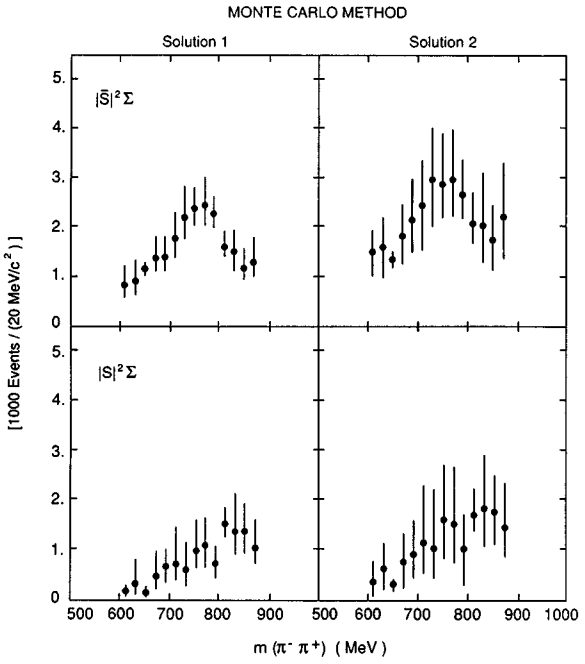

FIG. 1. Mass dependence of unnormalized amplitudes $|\overline{S}|^2\Sigma$ and $|S|^2\Sigma$ measured in $\pi^-p_\uparrow\to\pi^-\pi^+n$ at 17.2 GeV/c at $-t=0.005-0.20$ (GeV/c)^2 using the Monte Carlo method for amplitude analysis (Ref. [25]). Both solutions for the amplitude $|\overline{S}|^2\Sigma$ resonate at 750 MeV while the amplitude $|S|^2\Sigma$ is nonresonating in both solutions.

The results for the two solutions for the unnormalized moduli of S-wave amplitudes $|\overline{S}|^2\Sigma$ and $|S|^2\Sigma$ obtained by Monte Carlo amplitude analysis of CERN-Munich data at 17.2 GeV/c are shown in Fig. 1. We find that both solutions for the amplitude $|\overline{S}|^2\Sigma$ resonate around 750 MeV while both solutions for the amplitude $|S|^2\Sigma$ show nonresonant behavior and increase with dipion mass m.

The results for $|\overline{S}|^2\Sigma$ and $|S|^2\Sigma$ obtained by χ^2 minimization method using the same CERN-Munich data at 17.2 GeV are shown in Fig. 2. We again find that both solutions for the amplitude $|\overline{S}|^2\Sigma$ resonate around 750 MeV and that both solutions for the amplitude $|S|^2\Sigma$ show nonresonant behavior and an increase with dipion mass m. The comparison of Fig. 1 and Fig. 2 shows that the Monte Carlo method

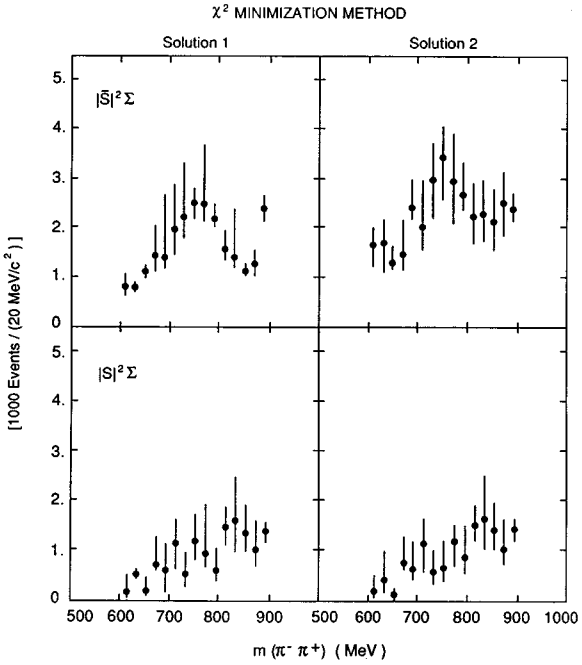

FIG. 2. Mass dependence of unnormalized amplitudes $|\overline{S}|^2\Sigma$ and $|S|^2\Sigma$ measured in $\pi^- p_\uparrow \to \pi^-\pi^+ n$ at 17.2 GeV/c at $-t=0.005-0.20$ (GeV/c)^2 using the χ^2 minimization method for amplitude analysis. Based on Fig. 10 of Ref. 4 and Fig. VI-21 of Ref. [3]. Both solutions for the amplitude $|\overline{S}|^2\Sigma$ resonate at 750 MeV while the amplitude $|S|^2\Sigma$ is nonresonating in both solutions. The analysis used the same data as in Fig. 1 (20 MeV mass bins).

and the χ^2 minimization method are also in excellent numerical agreement. However, the amplitudes obtained by the Monte Carlo method show a considerably smoother behavior which, as we shall see later, gives much lower χ^2 values in Breit-Wigner fits. The unnormalized moduli $|\overline{S}|^2\Sigma$ and $|S|^2\Sigma$ in Figs. 1 and 2 were calculated using $\Sigma = d^2\sigma/dmdt$ from Fig. 12 of Ref. [2].

At this point we note that the Fig. 2 is based on Fig. 10 of Ref. [4] and Fig. VI-21 of Ref. [3] (to resolve error bars). The authors of these papers present only normalized moduli $|\overline{S}|$ and $|S|$ and consequently did not see the resonant behavior of unnormalized amplitude $|\overline{S}|^2\Sigma$. The resonant behavior of amplitude $|S|^2\Sigma$ at 750 MeV went also unobserved in the subsequent analysis in Ref. [5] which was using polarized data in 40 MeV bins in the mass range from 600 to 1800 MeV. It is possible to reconstruct the amplitudes $|\overline{S}|^2\Sigma$ and $|S|^2\Sigma$ from the information given in Ref. [5]. As we shall see in Sec. V (Fig. 5) both solutions for $|\overline{S}|^2\Sigma$ resonate below 900 MeV while both solutions for $|S|^2\Sigma$ are nonresonating, in agreement with Figs. 1 and 2. It is interesting to note that the evidence for a narrow resonance $\sigma(750)$ was hidden in the very first analyses of CERN-Munich data (Refs. [3], [4], and [5]).

III. RESONANCE SHAPE FORMULAS

A. Pišút-Roos shape formula

Before we review the Pišút-Roos derivation of their resonance shape formula, we first recall some properties of partial waves in elastic scattering of scalar particles. The T-matrix amplitude of isospin I has partial wave expansion

$$T^I(s,\cos\theta) = 8\pi \sum_{L=0}^{\infty} (2L+1) T_L^I(s) P_L(\cos\theta). \quad (3.1)$$

The unitarity in elastic scattering then requires (see Ref. [28], pp. 38–40) that T_L^I has a form

$$T_L^I(s) = \frac{\sqrt{s}}{q} \sin\delta_L^I e^{i\delta_L^I} = \frac{\sqrt{s}}{q} \frac{1}{\mathrm{cotg}\,\delta_L^I - i}, \quad (3.2)$$

where q is the pion c.m.s. momentum and δ_L^I is the corresponding phase shift. Notice that the factor $\sqrt{s}/q$ is induced by the unitarity alone. At a resonance m_R, the relativistic Breit-Wigner formula for T_L^I then reads

$$T_L^I = \frac{\sqrt{s}}{q} \frac{-m_R\Gamma(s)}{(s-m_R^2)+im_R\Gamma(s)}, \quad (3.3)$$

where $\Gamma(s)$ is an energy-dependent width.

Let us now return to pion-production process $\pi^- p \to \pi^-\pi^+ n$ and to amplitudes $M^J_{\lambda\lambda_n,0\lambda_p}(s,t,m)$ defined in Eq. (2.8). In their analysis [26], Pišút and Roos assumed that the following amplitudes vanish for all J:

$$M^J_{0+,0+} = 0,$$

$$M^J_{\pm 1+,0+} = M^J_{\pm 1+,0-} = 0. \quad (3.4)$$

The conditions (3.4) mean that all A_1-exchange amplitudes vanish and that the natural A_2-exchange amplitudes also vanish. Only pion exchange amplitude $M^J_{0+,0-}$ contribute and they have a general form

$$M^J_{0+,0-}(s,t,m) = Q(s,t)\sqrt{2J+1}\,T^J(m)\sqrt{f(m)} + M^J_B(s,t,m), \quad (3.5)$$

where $T^J(m)$ are the $\pi\pi\to\pi\pi$ partial wave amplitudes with isospin decomposition

$$T^J = T^J_{I=1} \quad \text{for } J \text{ odd},$$

$$T^J = \frac{2}{3} T^J_{I=0} + \frac{1}{3} T^J_{I=2} \quad \text{for } J \text{ even}, \quad (3.6)$$

in reaction $\pi^+\pi^-\to\pi^+\pi^-$. In Eq. (3.5) the function $f(m)$ is a phenomenological function that is supposed to account for absorption, and initial-state and final-state interactions. In practice one puts $f(m)=1$. The function $Q(s,t)$ factorizes the s and t dependence. The term $M^J_B(s,t,m)$ is a background.

Taking into account the factor $qK(s)$ in Eq. (2.9) and Eq. (3.3), Pišút and Roos arrive at a resonant parametrization of the reaction cross section:

$$\frac{d^2\sigma}{dmdt} = q(2J+1)\left(\frac{m}{q}\right)^2 \frac{m_R^2\Gamma^2}{(m^2-m_R^2)^2+m_R^2\Gamma^2}\, f(m)\mathcal{N}(s,t) + \text{background terms}. \quad (3.7)$$

Averaging over t over an interval $\langle t_1,t_2\rangle$ gives a shape formula for the mass distribution:

$$I_{\rm av}(s,m)=q(2J+1)\left(\frac{m}{q}\right)^2 \frac{m_R^2\Gamma^2}{(m^2-m_R^2)^2+m_R^2\Gamma^2}\ f(m)N(s) + \text{background terms}, \tag{3.8}$$

where

$$I_{\rm av}(s,m)=\frac{1}{t_2-t_1}\int_{t_1}^{t_2}\frac{d^2\sigma(s,t,m)}{dmdt}\,dt,$$

$$N(s)=\frac{1}{t_2-t_1}\int_{t_1}^{t_2}\mathcal{N}(s,t)dt=\frac{K(s)}{t_2-t_1}\int_{t_1}^{t_2}|Q(s,t)|^2dt. \tag{3.9}$$

Setting $f(m)=1$ and ignoring the background we get the Pišút-Roos resonance shape formula [26] for the t-averaged mass distribution:

$$I_{\rm av}(m)=NqF(m)|A_{\rm BW}|^2, \tag{3.10}$$

where N is the normalization constant, q is the phase space factor, $F(m)$ is the Pišút-Roos shape factor,

$$F(m)=(2J+1)\left(\frac{m}{q}\right)^2=\frac{4(2J+1)}{1-\left(\frac{2\mu}{m}\right)^2}, \tag{3.11}$$

and $A_{\rm BW}$ is the Breit-Wigner amplitude

$$A_{\rm BW}=\frac{m_R\Gamma}{m_R^2-m^2-im_R\Gamma}. \tag{3.12}$$

The Pišút-Roos resonance shape formula (3.10) has been extensively used to fit partial wave intensities in previous amplitude analyses of $\pi N\to\pi^+\pi^-N$ on polarized targets (Refs. [5], [6], [7], and [25]). Averaging experimental data over different intervals of t (e.g., in adjacent t bins) will in general lead to mass distributions $I_{\rm av}(m)$ with some differences in the experimental resonance shape. These differences in $I_{\rm av}$ may result in differences in the values of resonance parameters determined in different t intervals using Eq. (3.10) to fit the averaged data. This problem was recognized already by Pišút-Roos in their paper [26].

B. Phenomenological resonance shape formula

In general, the experimental distribution $I(m)$ in a certain mass region is fitted to a functional form [27]

$$I(m)=\alpha_R I_R(m,m_R,\Gamma)+\alpha_B I_B(m), \tag{3.13}$$

where α_R and α_B give the fractions of resonant contribution and incoherent background. Normally I_R is taken as a square of the Breit-Wigner amplitude multiplied by a phase space factor. A coherent term may be added to the Breit-Wigner amplitude, typically a constant term. In general, the background $I_B(m)$ is a polynomial.

In the case of $\pi^-p\to\pi^-\pi^+n$ reaction, the relevant phase space factor is just the pion momentum q in the $\pi^+\pi^-$ c.m. system and one can write for mass distributions in this reaction a phenomenological resonance shape formula

$$I(m)=Nq(m)\{|A_{\rm BW}|^2+B\}, \tag{3.14}$$

where N is overall normalization factor and B is the background term. We can take $B=0$ or $B=$constant. When $B=0$, the phenomenological shape formula (3.14) is obtained from Pišút-Roos resonance shape formula (3.10) by setting their shape factor $F\equiv1$. We see from Eq. (3.11) that Pišút-Roos formula (3.10) converges to phenomenological formula (3.14) for large m when background $B=0$.

IV. THE MASS AND WIDTH OF $\sigma(750)$ FROM FITS TO THE S-WAVE AMPLITUDE $|\overline{S}|^2\Sigma$

As seen in Figs. 1 and 2, the Monte Carlo method and the χ^2 method yield very similar results for the S-wave amplitudes $|\overline{S}|^2\Sigma$ and $|S|^2\Sigma$ in $\pi^-p\to\pi^-\pi^+n$ at 17.2 GeV/c and for $-t=0.005-0.20$ (GeV/c)^2. Both methods show that the amplitude $|\overline{S}|^2\Sigma$ resonates in both solutions while the amplitude $|S|^2\Sigma$ is nonresonating in both solutions. The Monte Carlo results appear to be smoother than the χ^2 results. The Monte Carlo method found no physical solution at mass bin 890 MeV. The solution found by χ^2 method at this mass is far off from the general trend of data in solution 1 for $|\overline{S}|^2\Sigma$. For these reasons the mass bin 880–900 MeV was excluded from the fits to $|\overline{S}|^2\Sigma$.

To determine the best values of the mass and width of $\sigma(750)$ state from the mass distribution of the resonating amplitude $|\overline{S}|^2\Sigma$ we used four types of fitting approaches and used a χ^2 criterion to determine the best fits. In the first approach we used a single Breit-Wigner fit. In the second approach we added an incoherent constant background to the single Breit-Wigner. In the third and fourth approaches we used two different versions of constant coherent background. In each approach we used both Pišút-Roos and phenomenological resonance shape formula and found they give very similar results. The inclusion of background leads to the narrowing of the width of $\sigma(750)$. The best χ^2 solution is obtained by the fourth approach leading to a conclusion that $\sigma(750)$ is a narrow state with a width about 100 MeV. The fitting was done using the CERN optimization program FUMILI [33].

A. Single Breit-Wigner fit

In this approach the mass distribution $|\overline{S}|^2\Sigma$ is fitted to a formula

$$|\overline{S}|^2\Sigma=qFN_S|A_{\rm BW}|^2, \tag{4.1}$$

where q is the phase space factor (2.4). The factor F is equal either

$$F=(2J+1)\left(\frac{m}{q}\right)^2 \tag{4.2}$$

for Pišút-Roos shape formula or

$$F=1 \tag{4.3}$$

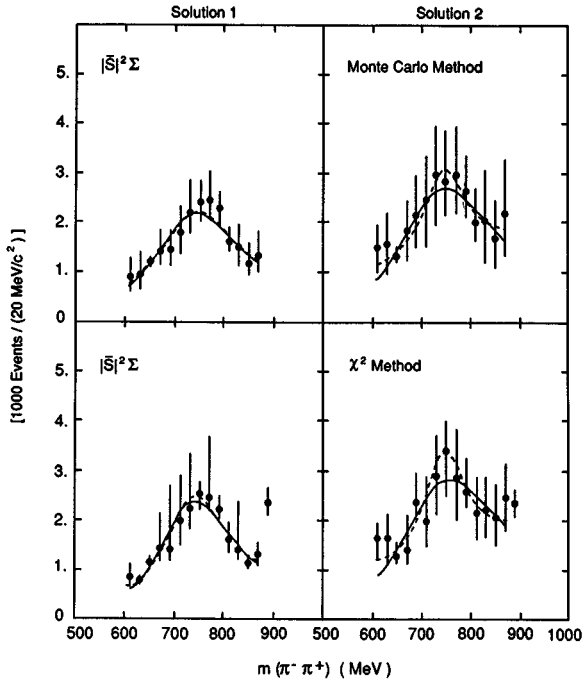

FIG. 3. The fits to amplitude $|\overline{S}|^2\Sigma$ using the single Breit-Wigner parametrization (4.1) with Pišút-Roos shape factor (4.2) and with phenomenological shape factor $F=1$. The two fits cannot be distinguished (solid line). The fitted parameters are given in Table I. The dashed lines represent fits to $|\overline{S}|^2\Sigma$ using the Breit-Wigner parametrization (4.7) with constant incoherent background and with phenomenological shape factor $F=1$. The fitted parameters are given in Table II.

for the phenomenological shape formula. $A_{\rm BW}$ is the Breit-Wigner amplitude

$$A_{\rm BW}=\frac{m_R\Gamma}{m_R^2-m^2-im_R\Gamma}, \tag{4.4}$$

where m_R is the resonant mass. The mass-dependent width $\Gamma(m)$ depends on spin J and has a general form

$$\Gamma=\Gamma_R\left(\frac{q}{q_R}\right)^{2J+1}\frac{D_J(q_Rr)}{D_J(qr)}. \tag{4.5}$$

In Eq. (4.5) $q_R=q(m=m_R)$ and D_J are the centrifugal barrier functions of Blatt and Weiskopf [34]:

$$D_0(qr)=1.0,$$

$$D_1(qr)=1.0+(qr)^2, \tag{4.6}$$

where r is the interaction radius.

The results of the fit are shown in Fig. 3 for the Pišút-Roos and phenomenological shape formulas. The corresponding curves (solid lines) for both shape formulas are nearly identical and cannot be distinguished in the figure. The numerical results are presented in Table I. The fits to $|\overline{S}|^2\Sigma$ obtained by χ^2 method have significantly higher values of $\chi^2/N_{\rm DF}$. However, both methods give a σ mass in the range 730–750 MeV and a width in the range 230–250 MeV. Only the solution 1 of the χ^2 method gives a lower width around 190 MeV.

TABLE I. Results of the fits to the mass distribution $|\overline{S}|^2\Sigma$ measured in $\pi^-p\to\pi^-\pi^+n$ at 17.2 GeV/c using a single Breit-Wigner formula (4.1). The notation MC and χ^2 indicates the solutions obtained by the Monte Carlo and χ^2 minimization methods, respectively.

$\lvert\overline{S}\rvert^2\Sigma$ Solution	m_σ (MeV)	Γ_σ (MeV)	N_σ	$\chi^2/N_{\rm DF}$
Pišút-Roos shape formula				
1(MC)	736±6	230±32	1.40±0.12	0.388
2(MC)	745±12	240±59	1.71±0.23	0.276
1(χ^2)	738±4	191±16	1.50±0.11	0.662
1(χ^2)	752±10	253±46	1.79±0.15	0.968
Phenomenological shape formula				
1(MC)	732±6	231±33	6.50±0.57	0.418
2(MC)	740±11	241±61	7.94±1.11	0.288
1(χ^2)	733±4	192±16	7.00±0.50	0.740
2(χ^2)	747±10	256±47	8.29±0.74	0.986

An important feature of the fits to $|\overline{S}|^2\Sigma$ with single Breit-Wigner formula noticeable in Fig. 3 is that all fits lie below the maximum values of the mass distributions for each solution and the method of analysis. This inability of the single Breit-Wigner formula to reproduce the resonant shape of the amplitude $|\overline{S}|^2\Sigma$ suggests that background contributions are important and their effect on the mass and width of σ state should be investigated, at least approximately.

B. Breit-Wigner fit with incoherent background

In this case we fit the mass distribution for $|\overline{S}|^2\Sigma$ to a formula

$$|\overline{S}|^2\Sigma=qFN_S\{|A_{\rm BW}|^2+B\}, \tag{4.7}$$

where B is the incoherent background added to the Breit-Wigner formula (4.1). In general, B is a polynomial in m. However, since we have only 14 data points in the resonant mass range of 600–880 MeV, we will take $B=$const.

The results of the fit are shown in Fig. 3 for the phenomenological shape formula (dashed lines). The results with Pišút-Roos shape formula are very similar. The numerical results are given in Table II. We notice a dramatic improvement of the fit to the solution 2 for both methods which yields a better $\chi^2/N_{\rm DF}$ and a narrow width of about 100 MeV. There is also some improvement of the fit to the solution 1 in particular for the χ^2 method solution. This improvement is again associated with a lower $\chi^2/N_{\rm DF}$ and a narrower width of 202 and 147 MeV for the Monte Carlo and χ^2 methods, respectively. The mass of the σ state remains in the range of 730–745 MeV.

While the fits to solutions 2 are now much improved, the fits to solutions 1 are still not satisfactory with the fitted curves still below the maximum values of these mass distributions. To make further progress we turn to coherent background contributions.

TABLE II. Results of the fits to the mass distribution $|\overline{S}|^2\Sigma$ measured in $\pi^- p \to \pi^- \pi^+ n$ at 17.2 GeV/c using a Breit-Wigner formula with a constant incoherent background (4.7). The notation MC and χ^2 as in Table I.

$\|\overline{S}\|^2\Sigma$ Solution	m_σ (MeV)	Γ_σ (MeV)	B	N_S	$\chi^2/N_{\rm DF}$
Phenomenological shape formula					
1(MC)	731± 6	202±110	0.15±0.55	5.75±2.54	0.416
2(MC)	744±14	103± 74	0.73±0.49	5.11±1.84	0.144
1(χ^2)	736± 4	147± 43	0.19±0.17	6.13±0.84	0.696
2(χ^2)	745±41	98± 41	0.70±0.28	5.70±1.30	0.626

C. Breit-Wigner fit with coherent background

The nonresonant behavior of the amplitude $|S|^2\Sigma$ (recoil nucleon transversity down) strongly suggest the presence of a coherent nonresonating background. A part of coherent background also comes from the contribution of isospin $I=2$ amplitudes [see Eq. (3.6)] which we neglected in the single Breit-Wigner fit. To understand the origins of the coherent background and to discuss its form for fits to $|S|^2\Sigma$ it is useful to express the unnormalized moduli of S-wave transversity amplitudes in terms of unnormalized helicity amplitudes. Using Eq. (2.13) we write

$$|S|^2\Sigma = \frac{1}{2}\ |S_0 + iS_1|^2\Sigma = qF|F_0 + iF_1|^2,$$

$$|\overline{S}|^2\Sigma = \frac{1}{2}\ |S_0 - iS_1|^2\Sigma = qF|F_0 - iF_1|^2, \qquad (4.8)$$

where F_0 and F_1 are unnormalized S-wave helicity amplitudes. The terms qF have the same meaning as in Eq. (4.1) and anticipate the use of Eq. (4.8) for Breit-Wigner fits to mass distribution of $|\overline{S}|^2\Sigma$. Near the resonance with mass m_R we assume the following form of the helicity amplitudes

$$F_n(s,t,m) = R_n(s,t,m)A_{\rm BW}(m) + B_n(s,t,m), \qquad (4.9)$$

where $n=0,1$ is the nucleon helicity flip, $A_{\rm BW}$ is the Breit-Wigner amplitude (4.4), $R_n(s,t,m)$ is the pole term, and $B_n(s,t,m)$ is the nonresonating background which includes the contribution from the nonresonating isospin $I=2$ amplitudes. The energy variable s is fixed and will be omitted in the following. Since the experimental mass distributions are averaged over broad t bins, we will eventually average also over the momentum transfer variable t. With the notation $\epsilon = \pm 1$, we can then write Eq. (4.8) in a compact form as

$$F_0 + i\epsilon F_1 = R_\epsilon(t,m)A_{\rm BW}(m) + B_\epsilon(t,m), \qquad (4.10)$$

where $R_\epsilon = R_0 + i\epsilon R_1$ and $B_\epsilon = B_0 + i\epsilon B_1$. It is useful to factor out the phase of R_ϵ and define

$$R_\epsilon = |R_\epsilon| e^{i\phi_\epsilon},$$

$$C_\epsilon = B_\epsilon e^{-i\phi_\epsilon}. \qquad (4.11)$$

Then Eq. (4.10) takes the form

$$F_0 + i\epsilon F_1 = \{|R_\epsilon| A_{\rm BW} + C_\epsilon\} e^{i\phi_\epsilon} \qquad (4.12)$$

and the moduli squared of Eq. (4.8) read

$$|F_0 + i\epsilon F_1|^2 = |R_\epsilon|^2 |A_{\rm BW}|^2 + ({\rm Re}C_\epsilon)^2 + ({\rm Im}C_\epsilon)^2 + 2|R_\epsilon|\{{\rm Re}C_\epsilon\ {\rm Re}\ A_{\rm BW} + {\rm Im}C_\epsilon\ {\rm Im}A_{\rm BW}\}. \qquad (4.13)$$

We now recall that

$${\rm Re}A_{\rm BW} = \left(\frac{m_R - m^2}{m_R\Gamma}\right)|A_{\rm BW}|^2 \equiv w|A_{\rm BW}|^2$$

$${\rm Im}A_{\rm BW} = |A_{\rm BW}|^2. \qquad (4.14)$$

Hence,

$$|F_0 + i\epsilon F_1|^2 = \{|R_\epsilon|^2 + 2|R_\epsilon|{\rm Re}C_\epsilon w + 2|R_\epsilon|{\rm Im}C_\epsilon\}|A_{\rm BW}|^2 + ({\rm Re}C_\epsilon)^2 + ({\rm Im}C_\epsilon)^2. \qquad (4.15)$$

Since the amplitude $|S|^2\Sigma(\epsilon=+1)$ does not show a clear resonant behavior (Figs. 1 and 2), we can conclude from Eq. (4.15) that the sum of terms in the parentheses must be small or zero. This most likely means that $|R_+|$ is small or zero implying that the pole terms in helicity amplitudes are related approximately as $R_0 \approx -iR_1$.

For the resonating amplitude $|\overline{S}|^2\Sigma(\epsilon=-1)$ the second and third terms in the parentheses in Eq. (4.15) represent the effect of coherent background. In general the functions $|R_-|$ and C_- will depend on both t and m. Since these functions are not known and since we have only 14 data points in the resonance mass region 600–880 MeV, we will work in the approximation of constant background. At this point there are two possibilities.

(1) We assume that $|R_-|$ and C_- are constants independent of t and m. In this case no averaging over t is necessary and we can write Eq. (4.15) in the form

$$|\overline{S}|^2\Sigma = qFN_S\{[1 + 2wB_1 + 2B_2]|A_{\rm BW}|^2 + B_1^2 + B_2^2\}, \qquad (4.16)$$

where

$$N_S = |R_-|^2, \quad B_1 = \frac{{\rm Re}C_-}{|R_-|}, \quad B_2 = \frac{{\rm Im}C_-}{|R_-|}. \qquad (4.17)$$

This possibility is equivalent to assuming that the constant parts of $|R_-|$ and C_- dominate in the resonant mass range 600–880 MeV. We also notice that in this case the incoherent part $B_1^2 + B_2^2$ is correlated with the coherent contribution

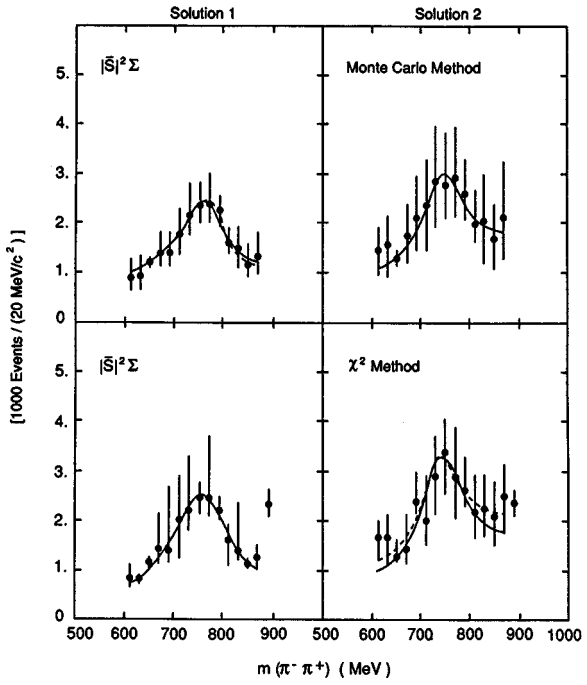

FIG. 4. The fits to amplitude $|\overline{S}|^2\Sigma$ using the Breit-Wigner parametrization (4.16) with constant coherent background and with phenomenological shape factor $F=1$ (solid lines). The fitted parameters are given in Table III. The dashed lines represent the fits to amplitude $|\overline{S}|^2\Sigma$ using the Breit-Wigner parametrization (4.20) with t-averaged constant coherent background and with phenomenological shape factor $F=1$. The fitted parameters are given in Table IV.

$(2wB_1+2B_2)|A_{\rm BW}|^2$ in the formula (4.16) through the common parameters B_1 and B_2.

(2) In the second possibility, we assume that $|R_-|$ and C_- are both dependent on t and m. In this case we must average Eq. (4.15) over t over the experimentally measured interval $\langle t_1,t_2\rangle$. The averaging of Eq. (4.15) over t yields

$$|\overline{S}|^2\Sigma = qF\{[r+2wa+2b]|A_{\rm BW}|^2+c\}, \qquad (4.18)$$

where

$$r=\langle|R_-|^2\rangle, \quad a=\langle|R_-|{\rm Re}C_-\rangle,$$
$$b=\langle|R_-|{\rm Im}C_-\rangle, \quad c=\langle({\rm Re}C_-)^2+({\rm Im}C_-)^2\rangle. \qquad (4.19)$$

In Eq. (4.19) the symbol $\langle\rangle$ represents averaging over t over interval $\langle t_1,t_2\rangle$. In general, the functions r,a,b,c will depend on the mass m. Since we do not know these functions, we will assume constant values. But then there is no distinction between r and $2b$ which can be combined into one parameter $N_S=r+2b$ as they are two constants in a sum. Then Eq. (4.18) has the form

$$|\overline{S}|^2\Sigma = qFN_S\{[1+2wB_1]|A_{\rm BW}|^2+B\}, \qquad (4.20)$$

where $B_1=a/N_S$ and $B=c/N_S$ are the coherent and incoherent contributions to the resonance shape formula. This approximation is equivalent to assumption that the functions $|R_-|$ and C_- depend mostly on t and only weakly on m. Notice that in this case the incoherent contribution B is not correlated with the coherent contribution as the parameters B and B_1 are independent. We will refer to the first possibility (1) as Breit-Wigner fit with constant coherent background and to the second possibility (2) as the Breit-Wigner fit with t-averaged constant coherent background.

The results of the Breit-Wigner fit with constant coherent background are shown in Fig. 4 (solid lines) and Table III. The results of the Breit-Wigner fit with the t-averaged constant coherent background are given in Fig. 4 (dashed lines where distinguishable from the solid lines) and Table IV. Both figures and tables refer to the phenomenological shape formula with $F=1$. The results with Pišút-Roos resonance shape formula [F given by Eq. (4.2)] are very similar for the masses and widths although there are some differences in the fitted values of the constants B_1, B_2, or B_1 and B.

An inspection of Fig. 4 shows much improved fits to the data on mass distribution of $|\overline{S}|^2\Sigma$. The overall best fit (as judged by the lowest values of $\chi^2/N_{\rm DF}$) is provided by the Breit-Wigner fit with the t-averaged constant coherent background. However, the improvements in $\chi^2/N_{\rm DF}$ appear only in solution 1 of Monte Carlo method and solution 2 of the χ^2 method. Again, the Monte Carlo method achieves better values of $\chi^2/N_{\rm DF}$ compared to the χ^2 method of amplitude analysis.

The improvements in the fits brought about by the inclusion of coherent background have important consequences for the fitted values of the mass and width of $\sigma(750)$ state. From Tables III and IV we find that the mass of σ in solution 1 is about 30 MeV higher than the σ mass found in solution 2. The Monte Carlo method gives the best value of σ mass 774 MeV in solution 1 and 744 MeV in solution 2 (Table IV). The χ^2 method gives the best value of σ mass 761 MeV in solution 1 and 733 MeV in solution 2 (Table IV). The data on polarized target cannot distinguish these two solutions. Since the two masses are close, we can work with a solution

TABLE III. Results of the fits to the mass distribution $|\overline{S}|^2\Sigma$ measured in $\pi^-p\to\pi^-\pi^+n$ at 17.2 GeV/c using a Breit-Wigner formula with constant coherent background (4.16). The notation MC and χ^2 as in Table I.

$\|\overline{S}\|^2\Sigma$ Solution	m_σ (MeV)	Γ_σ (MeV)	B_1	B_2	N_S	$\chi^2/N_{\rm DF}$
Phenomenological shape formula						
1(MC)	770±19	114±17	0.90±0.43	1.34±0.84	1.09±0.61	0.136
2(MC)	745±31	104±76	0.02±1.07	1.84±1.14	1.09±0.90	0.144
1(χ^2)	761±13	138±19	0.34±0.16	0.69±0.45	2.41±1.14	0.362
2(χ^2)	738±20	103±112	−0.17±0.65	1.30±0.50	1.79±0.86	0.898

TABLE IV. Results of the fits to the mass distribution $|\overline{S}|^2\Sigma$ measured in $\pi^- p \to \pi^- \pi^+ n$ at 17.2 GeV/c using a Breit-Wigner formula with t-averaged constant coherent background (4.20). The notation MC and χ^2 as in Table I.

$\lvert\overline{S}\rvert^2\Sigma$ Solution	m_σ (MeV)	Γ_σ (MeV)	B	B	N_S	$\chi^2/N_{\rm DF}$
Phenomenological shape formula						
1(MC)	774±14	101±44	0.73±0.31	0.29±0.14	3.99±0.96	0.108
2(MC)	744±31	103±79	0.73±0.54	0.01±0.23	5.10±1.90	0.144
1(χ^2)	761±12	134±41	0.25±0.17	0.15±0.07	5.74±0.82	0.362
2(χ^2)	733±20	93±48	0.80±0.39	−0.12±0.19	5.31±1.53	0.592

average. The solution average for σ mass is 759±22 MeV for Monte Carlo method and 747±16 MeV for the χ^2 method. The average over the two methods gives σ mass 753±19 MeV.

The most significant effect of the inclusion of coherent background is the reduction of the value of the width of σ. The Monte Carlo method gives for the best value of σ width similar values of 101 and 103 MeV in solutions 1 and 2, respectively (Table IV). The χ^2 method gives for the best value of σ width 134 MeV in solution 1 and 93 MeV in solution 2 (Table IV). The data on polarized target cannot distinguish these two solutions, but the high values of $\chi^2/N_{\rm DF}$ for χ^2 method tend to favor the values for σ width from the Monte Carlo method which has low values of $\chi^2/N_{\rm DF}$. The solution average for the σ width is 102±61 MeV for Monte Carlo method. The solution average for the σ width is 113±44 MeV for the χ^2 method. Since the error on the σ width is larger for the Monte Carlo method, the two results are essentially compatible. The average over the two methods gives σ width 108±53 MeV.

In conclusion, we propose to adopt the solution and method averages from the best fit values of Table IV as the standard values of mass and width of the σ state. The obtained values are

$$m_\sigma = 753 \pm 19 \ \text{MeV}, \quad \Gamma_\sigma = 108 \pm 53 \ \text{MeV}. \quad (4.21)$$

V. THE INTERFERENCE WITH $f_0(980)$ IN FITS TO AMPLITUDE $|S|^2\Sigma$

Törnqvist suggested [35,36] that the interference of $\sigma(750)$ with $f_0(980)$ resonance could influence the determination of resonance parameters of $\sigma(750)$. In the old phase shift analyses (obtained using the invalid assumption of absence of A_1 exchange), the resonance $f_0(980)$ plays an important role of smoothly interpolating the ''down'' solution for δ_0^0 below 900 MeV with the results for δ_0^0 above 1000 MeV.

We will now investigate the effect of interference of $\sigma(750)$ with $f_0(980)$ on the determination of resonance parameters of $\sigma(750)$. We will find that the effect is very small. This is consistent with the fact that $f_0(980)$ is a very narrow resonance and it is positioned sufficiently far away from the narrow and strong resonance $\sigma(750)$.

The experimental data in the $f_0(980)$ mass region are given in the CERN-Munich analysis [5] of $\pi^- p \to \pi^- \pi^+ n$ on polarized target at 17.2 GeV/c for dipion masses 600–1800 MeV. From Fig. 2 and Fig. 6 of Ref. [5] it is possible to reconstruct the amplitudes $|\overline{S}|^2\Sigma$ and $|S|^2\Sigma$. The two solutions are shown in Fig. 5. The amplitude $|S|^2\Sigma$ resonates at 750 MeV in solution 1 and at 800 MeV in solution 2. It shows a high value at 960 MeV and a pronounced dip at 1000 MeV, indicating an interference of $f_0(980)$ with background in this mass region around 1000 MeV. The structures are less dramatic in $|S|^2\Sigma$ which does not show $\sigma(750)$ but a dip at 1000 MeV is still observable.

To proceed, we extend our parametrization (4.9) of $|\overline{S}|^2\Sigma$ to include $f_0(980)$ resonance. Recall from Eq. (4.8) that $|\overline{S}|^2\Sigma = qF|F_0 - iF_1|$. Now we write, for the helicity amplitudes F_0 and F_1,

$$F_n = R_n^{(\sigma)}(s,t,m) A_{\mathrm{BW}\sigma}(m) + R_n^{(f)}(s,t,m) A_{\mathrm{BW}f}(m) + B_n(s,t,m), \quad (5.1)$$

where index σ refers to $\sigma(750)$ and f refers to $f_0(980)$. Then

$$F_0 - iF_1 = R_\sigma(s,t,m) A_{\mathrm{BW}_\sigma} + R_f(s,t,m) A_{\mathrm{BW}_f} + B(s,t,m). \quad (5.2)$$

Assuming that the coefficients R_σ, R_f and the background B are independent of t and m, we get an extension of the parametrization (4.16):

$$|\overline{S}|^2\Sigma = qFN_S\{[1 + 2w_\sigma B_1 + 2B_2]|A_{\mathrm{BW}_\sigma}|^2 + B_1^2 + B_2^2 + [C_1^2 + C_2^2]|A_{\mathrm{BW}_f}|^2 + 2[(w_\sigma |A_{\mathrm{BW}_\sigma}|^2 + B_1)(w_f C_1 - C_2) + (|A_{\mathrm{BW}_\sigma}|^2 + B_2)(C_1 + w_f C_2)]|A_{\mathrm{BW}_f}|^2\}, \quad (5.3)$$

where

$$w_R = \frac{m_R^2 - m^2}{m_R \Gamma}, \quad \Gamma = \Gamma_R\left(\frac{q}{q_R}\right), \quad R = \sigma, f. \quad (5.4)$$

If we assume that R_σ, R_f, and B depend on t and perform t averaging, the extension of parametrization (4.20) then reads

$$|\overline{S}|^2\Sigma = qFN_S\{[1 + 2w_\sigma B_1]|A_{\mathrm{BW}_\sigma}|^2 + B + 2[w_\sigma(w_f C_1 - C_2) + (C_1 + w_f C_2)]|A_{\mathrm{BW}_f}|^2 |A_{\mathrm{BW}_\sigma}|^2 + (D_1 + w_f D_2)|A_{\mathrm{BW}_f}|^2\}. \quad (5.5)$$

In the above parametrizations (5.3) and (5.5) the coefficients N_S, B_1, B_2, (B), C_1, C_2, D_1, D_2 are real constants. The

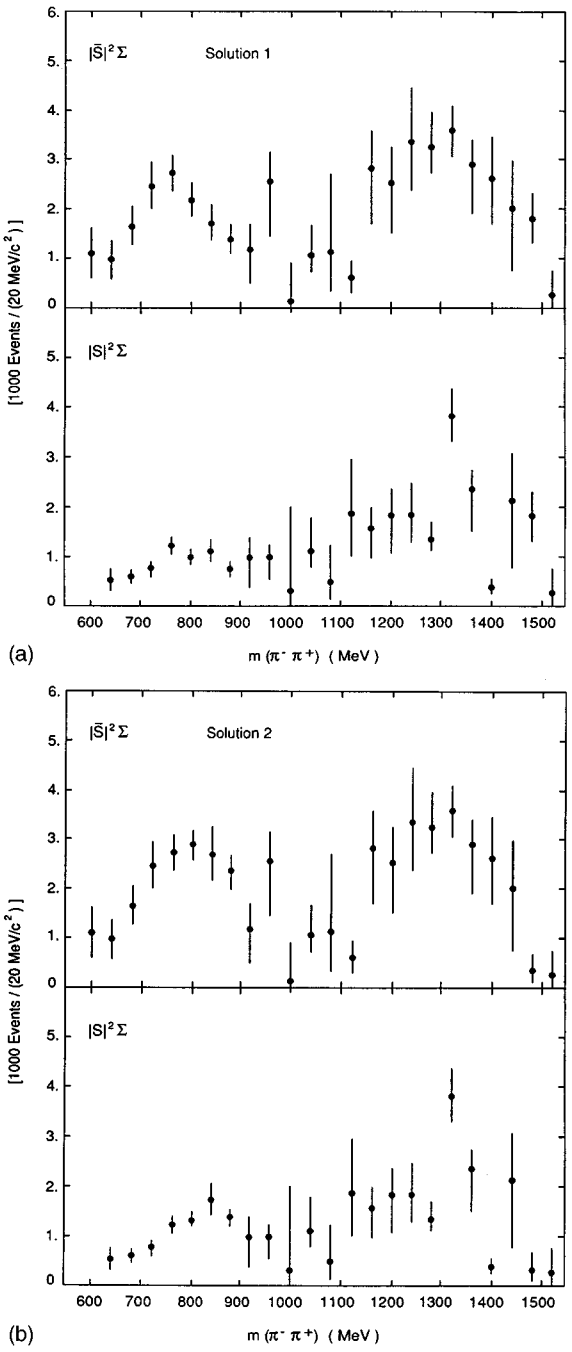

FIG. 5. Mass dependence of unnormalized amplitudes $|\overline{S}|^2\Sigma$ and $|S|^2\Sigma$ measured in $\pi^- p \to \pi^- \pi^+ n$ at 17.2 GeV/c at $-t = 0.005 - 0.20$ (GeV/c)^2 in 40 MeV mass bins from 600 to 1520 MeV. Based on Figs. 2 and 6 from Ref. [5]. The amplitude $|S|^2\Sigma$ resonates at 750 in solution 1 and at 800 MeV in solution 2 while the amplitude for $|S|^2\Sigma$ is nonresonating in both solutions in this mass range.

data between 900 and 1120 MeV exist only in 40 MeV mass bins. Thus there is not enough data to fit the resonance parameters of $f_0(980)$. Instead we fix the mass of $f_0(980)$ at 980 MeV and its width at 48 MeV in the Breit-Wigner amplitude A_{BW_f}. Also, in our fits we took for $|S|^2\Sigma$ below 880 MeV the results from our Monte Carlo analysis (in 20 MeV bins) and between 900 and 1120 MeV we took the results of CERN-Munich analysis (in 40 MeV bins) from Fig. 5.

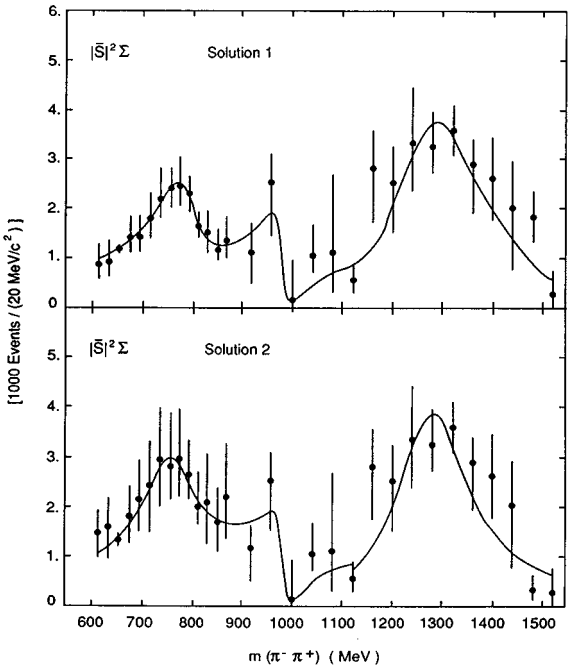

FIG. 6. The fits to amplitude $|\overline{S}|^2\Sigma$ using the Breit-Wigner parametrization (5.3) below 1120 MeV and a single Breit-Wigner formula with incoherent background above 1120 MeV. The phenomenological shape factor $F=1$. The fitted parameters are given in Tables V and VI.

The two parametrizations (5.3) and (5.5) yield virtually identical fits from 600 to 1120 MeV and the same values for mass and width of $\sigma(750)$. The fit for parametrization (5.3) is shown in Fig. 6 and the numerical values of the parameters are given in Table V. There is a small improvement of χ^2/N_{DF} in Solution 1 which shows a better fit with the $f_0(980)$ interference. Comparison with the corresponding Table III shows a small increase in the mass of σ in both solutions. There is a decrease of the σ width in solution 1 from 114 to 95 MeV and an increase in σ width in Solution 2 from 104 to 135 MeV. The solution averages are

$$m_\sigma = 768 \pm 22 \ \text{MeV}, \quad \Gamma_\sigma = 115 \pm 38 \ \text{MeV}. \tag{5.6}$$

The effect of $f_0(980)$ interference is thus a small increase of average mass and width of σ as compared to values in Eq. (4.21). It is not possible to claim [36] that the low mass and the narrow width of $\sigma(750)$ can be explained by the neglect of interference of $\sigma(750)$ with $f_0(980)$ in our fits.

Both fits reproduce well the σ resonance peaks below 880 MeV in both solutions and the interference patterns between 920 and 1120 MeV. Particularly noteworthy in Fig. 6 is the dramatic drop in $|S|^2\Sigma$ between 960 and 1000 MeV due to destructive interference of $f_0(980)$ with the background. The good fit in this region suggests that the assumption of constant coherent background and resonance couplings is a good approximation.

We have also attempted to fit the whole mass region of 600–1520 MeV using a three resonance parametrization with a constant background and resonance couplings. The fit was not successful as the $f_0(1300)$ resonance was not well reproduced. This indicates that the background above 1120 MeV

TABLE V. Results of the fit to the mass distribution $|\overline{S}|^2\Sigma$ in the mass range from 600 to 1120 MeV taking into account the interference of $\sigma(750)$ with $f_0(980)$ using the parametrization (5.3). The notation MC and χ^2 as in Table I.

$\lvert\overline{S}\rvert^2\Sigma$ Solution	m_σ (MeV)	Γ_σ (MeV)	B_1	B_2	N_S	$\chi^2/N_{\rm DF}$
Phenomenological shape formula						
1(MC,χ^2)	778±13	95±27	1.20±0.35	0.85±0.33	1.24±0.39	0.096
2(MC,χ^2)	758±32	135±49	0.54±0.69	1.00±0.28	1.85±0.83	0.162
			C_1	C_2		
1(MC,χ^2)			0.42±0.52	1.25±0.39		
2(MC,χ^2)			−0.35±0.67	0.97±0.55		

is different and the assumption of constant background for such a large mass range does not work. Next we fitted the $f_0(1300)$ resonance in the mass range of 1120 to 1520 MeV to a single Breit-Wigner with incoherent background. The results are shown in Fig. 6 for the two solutions (differing in values of $|\overline{S}|^2\Sigma$ at 1480 MeV). The Solution 1 above 1120 MeV connects smoothly with both solutions below 1120 MeV while the Solution 2 shows a small discontinuity at 1120 MeV. Surprisingly, the incoherent background in both solutions is consistent with zero. This again indicates that above 1100–1200 MeV the background (if any) is different from the low mass region below 1100 MeV. The numerical results of the fit to $f_0(1300)$ in the mass region 1120–1520 MeV are given in Table VI. We note the similarity of mass and width of resonances $f_0(1300)$ and $f_2(1270)$.

VI. THE MASS AND WIDTH OF $\sigma(750)$ STATE FROM THE FITS TO S-WAVE INTENSITY I_S

Previous amplitude analyses [4–6,25] of $\pi^- p\to\pi^-\pi^+ n$ and $\pi^+ n\to\pi^+\pi^- p$ data on polarized targets fitted only certain partial wave intensities using the Pišút-Roos resonance shape formula without any background. It is of interest to perform Breit-Wigner fits to the S-wave intensity I_S and compare the results with the results of fits to resonating amplitude $|\overline{S}|^2\Sigma$ in $\pi^- p\to\pi^-\pi^+ n$ at 17.2 GeV/c. Because of lower statistics, data for $\pi^+ n\to\pi^+\pi^- p$ at 5.98 and 11.85 GeV/c allow fits only to S-wave intensity I_S. This is, thus, our primary aim in fitting the S-wave intensity: to extract information about the mass and width of σ in $\pi^+ n\to\pi^+\pi^- p$ reaction measured at larger momentum transfers $-t=0.2$–0.4 $(\mathrm{GeV}/c)^2$.

Let us recall that the S-wave intensity I_S is defined as

$$I_S(s,t,m)=(|S|^2+|\overline{S}|^2)\Sigma=(|S_0|^2+|S_1|^2)\Sigma. \quad (6.1)$$

Since there are two independent solutions for the amplitudes $|S|^2$ and $|\overline{S}|^2$, there are four solutions for the S-wave intensity. We label these four solutions as $I_S(1,1)$, $I_S(1,2)$, $I_S(2,1)$, and $I_S(2,2)$, where

$$I_S(i,j)=(|S(i)|^2+|\overline{S(j)}|^2)\Sigma, \quad i,j=1,2. \quad (6.2)$$

The results for the four solutions of I_S obtained by the Monte Carlo amplitude analysis are shown in Fig. 7. The results for $I_S(1,1)$ and $I_S(2,2)$ obtained by the χ^2 minimization method are shown in Fig. 8. Again, there is a remarkable agreement between the results of these two different methods of analysis. The solutions $I_S(1,1)$ and $I_S(2,1)$ are clearly resonating but the solutions $I_S(1,2)$ and $I_S(2,2)$ do not show a clear resonant behavior. This is due to the large nonresonating contribution from the amplitude $|S|^2\Sigma$ (see Figs. 1 and 2). The amplitude $|S|^2\Sigma$ represents a nontrivial nonresonating background in all four solutions and is thus expected to distort the results of Breit-Wigner fits to I_S.

We first performed fits to I_S using a single Breit-Wigner formula without any background

$$I_S=qFN_S|A_{\rm BW}|^2. \quad (6.3)$$

In all fits to S-wave intensities we used the Pišút-Roos shape factor $F=(2J+1)(m/q)^2$. The results are shown as solid lines in Figs. 7 and 8 and in Tables VII and Tables VIII for the Monte Carlo and χ^2 methods, respectively. We notice in Figs. 7 and 8 that the single Breit-Wigner fit is well below the maximum values of the mass distribution I_S. In the Monte Carlo analysis the mass of σ is around 766 MeV in all four solutions. The width is around 260 MeV for the first three solutions and is larger at 303 MeV for the solutions $I_S(2,2)$. In the χ^2 method the σ mass and width in solution $I_S(1,1)$ is in agreement with the Monte Carlo results, but the width of $I_S(2,2)$ is larger at 408 MeV and also the mass is higher at 786 MeV.

TABLE VI. The results of the fit to the mass distribution $|\overline{S}|^2\Sigma$ in the $f_0(1300)$ mass region from 1120 to 1520 MeV using a single Breit-Wigner formula with incoherent constant background. The notation χ^2 as in Table I.

$\lvert\overline{S}\rvert^2\Sigma$ Solution	m (MeV)	Γ (MeV)	B	N	$\chi^2/N_{\rm DF}$
1(χ^2)	1284±12	209±29	0.001±0.32	5.96±0.62	1.393
2(χ^2)	1276±11	175±24	0.001±0.09	6.21±0.70	1.738

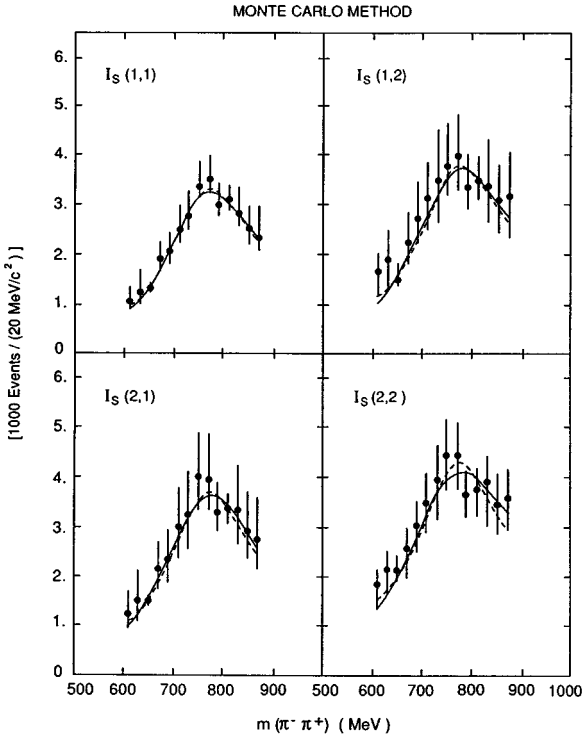

FIG. 7. Four solutions for the S-wave intensity I_S measured in the reaction $\pi^- p_\uparrow \to \pi^-\pi^+ n$ at 17.2 GeV/c and $-t = 0.005-0.2$ (GeV/c)^2 using the Monte Carlo method for amplitude analysis (Ref. [25]). The solid curves are fits to single Breit-Wigner parametrization (6.3). The dashed curves are fits to Breit-Wigner parametrization (6.4) with incoherent background. The fitted parameters are given in Table VII.

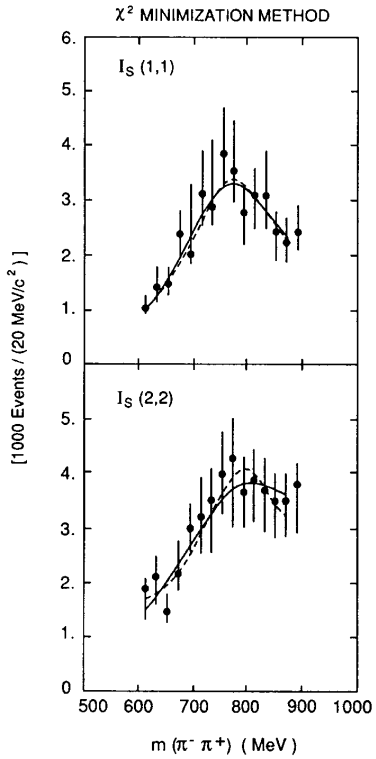

FIG. 8. Two of the four solutions for the S-wave intensity I_S measured in the $\pi^- p_\uparrow \to \pi^-\pi^+ n$ at 17.2 GeV/c and $-t = 0.005-0.2$ (GeV/c)^2 using the χ^2 minimization method for amplitude analysis. The data are based on Fig. 14(a) of Ref. [4] and Fig. 12 of Ref. [2]. The solid and dashed curves are Breit-Wigner fits as in Fig. 7. The fitted parameters are given in Table VIII.

Next we performed a Breit-Wigner fit with a constant incoherent background using the formula

$$I_S = qFN_S\{|A_{\rm BW}|^2 + B\}, \tag{6.4}$$

where B is the constant background term. The results are shown as dashed lines in Figs. 7 and 8 and in Tables VII and VIII for the Monte Carlo and χ^2 methods, respectively. While the masses of σ remain the same, there is a general reduction of the width of σ associated with improved fits to the data and lower values of $\chi^2/N_{\rm DF}$. In Monte Carlo method the width of σ is reduced to 210 MeV in the first three solutions to I_S. However, the most dramatic and unexpected change occurs in the solution $I_S(2,2)$ in both methods. There is a considerable improvement in the fit to the data and the width is drastically reduced to 188 MeV in both methods indicating the existence of a narrow σ state even in the broad looking mass distribution.

The best determination of σ width from the fits to S-wave intensity I_S is still double the best value obtained in fits directly to the amplitude $|\overline{S}|^2\Sigma$ (Table IV). This discrepancy shows that the determination of resonance parameters from the spin-averaged intensities is not fully reliable when there is a presence of a large nonresonating nontrivial background as is the case of the amplitude $|S|^2\Sigma$. The characteristic feature of this situation is that the S-wave intensity does not show a clear resonant structure in all four solutions.

This situation does not occur in the data on S-wave intensity in $\pi^+ n \to \pi^+\pi^- p$ at larger momentum transfers $-t = 0.2-0.4$ (GeV/c)^2. The results from Monte Carlo amplitude analysis are shown in Figs. 9 and 10 at 5.98 and 11.85 GeV/c, respectively. We note that all four solutions at both energies show clear resonant structures. This suggests that the determination of resonance parameters from S-wave intensities at these momentum transfers should be more reliable. However, this advantage is somewhat offset by the lower statistics of the data and large errors.

We have again performed fits using single Breit-Wigner formula (6.3) and the Breit-Wigner fit with constant incoherent background using formula (6.4). The results are shown in Figs. 9 and 10 and in Table IX and Table X for incident momenta of 5.98 and 11.85 GeV/c, respectively. The fit with constant background (dashed lines) is a clear improvement over a single Breit-Wigner fit (solid lines). The improvement of the fit with the constant background is again associated with lower values of $\chi^2/N_{\rm DF}$ and with reduction of the width of σ in all solutions at both energies. However, there are differences in values for the mass and the width of σ between the solutions as well as between energies. At 5.98 GeV/c, the mass ranges from 706 to 745 MeV and the width ranges from 145 to 262 MeV. At 11.85 GeV/c, the mass is higher and ranges from 756 to 782 MeV while the width is lower ranging from 117 to 202 MeV. The differences are probably due to lower statistics.

TABLE VII. Results of the fits to the four solutions of the S-wave intensity measured in $\pi^- p \to \pi^- \pi^+ n$ at 17.2 GeV/c using the Monte Carlo method for amplitude analysis. The fits are made with Breit-Wigner parametrization (6.3) and Eq. (6.4) with the Pišút-Roos shape factor.

I_S Solution	m_σ (MeV)	Γ_σ (MeV)	B	N_S	$\chi^2/N_{\rm DF}$
Single Breit-Wigner fit					
(1,1)	766±5	258±19		1.98±0.07	0.450
(1,2)	769±12	263±45		2.26±0.17	0.498
(2,1)	766±10	255±37		2.19±0.15	0.240
(2,2)	768±12	303±49		2.48±0.16	0.816
Breit-Wigner fit with constant background					
(1,1)	767±5	210±431	0.19±0.17	1.69±0.23	0.365
(1,2)	768±12	209±99	0.20±40	1.92±0.61	0.470
(2,1)	766±9	208±82	0.17±0.32	1.91±0.47	0.218
(2,2)	765±10	188±76	0.41±0.34	1.85±0.42	0.700

The solution averages for the mass and width of σ from fits to I_S are as follows. At 5.98 GeV/c

$$m_\sigma = 730 \pm 27 \ \text{MeV}, \quad \Gamma_\sigma = 195 \pm 81 \ \text{MeV}. \tag{6.5}$$

At 11.85 GeV/c

$$m_\sigma = 768 \pm 17 \ \text{MeV}, \quad \Gamma_\sigma = 166 \pm 54 \ \text{MeV}. \tag{6.6}$$

At 17.2 GeV/c

$$m_\sigma = 767 \pm 9 \ \text{MeV}, \quad \Gamma_\sigma = 204 \pm 75 \ \text{MeV}. \tag{6.7}$$

The best values for the mass and width of σ obtained from fits to the S-wave intensities at the three energies are in general agreement. The small differences are likely due to the fact that the approximation of constant incoherent background may work differently at various energies and momentum transfers. The differences in mass of σ from the fits to $\overline{|S|^2}\Sigma$ and to I_S are small. The difference in the value of the width from the best fits to $\overline{|S|^2}\Sigma$ with coherent background and the fits to I_S are somewhat large but the results are still consistent. At 17.2 GeV/c they are due to large nonresonating contributions from the amplitude $\overline{|S|^2}\Sigma$. The differences also reflect the need for the inclusion of coherent background and a better description than a constant. This in turn would require more data of high statistics in the resonance region 600–900 MeV.

VII. REMARKS ON THE DETERMINATIONS OF $\pi\pi$ PHASE SHIFTS

The amplitude analyses of measurements of $\pi N_\uparrow \to \pi^+ \pi^- N$ on polarized targets provide model-independent and solution-independent evidence for a narrow scalar state $I=0 \ 0^{++}(750)$. The question of how to understand the absence of such a state in the conventional S-wave phase shift δ_0^0 in $\pi\pi$ scattering arises [2,13–19].

Of course, there are no actual measurements of pion-pion scattering and there is no partial-wave analysis of $\pi\pi \to \pi\pi$ reactions in the usual sense. The $\pi\pi$ phase shifts are determined indirectly from measurements of $\pi^- p \to \pi^- \pi^+ n$ on unpolarized targets using several strong enabling assumptions. One of these crucial assumptions—the absence of A_1 exchange amplitudes—leads to predictions for polarized spin density matrix (SDM) elements and for the measured amplitudes, and it is thus directly testable in the measurements on polarized targets. As we shall see below, the assumption of an absence of A_1-exchange amplitudes is totally invalidated by the data on polarized targets. The polarization measurements also cast some doubt on the fundamental assumption of factorization of mass m and momentum transfer t in the crucial pion exchange amplitudes. We must use the results of the measurements on polarized targets to judge the validity of $\pi\pi$ phase shifts, and not vice versa. We are thus led to the conclusion that the indirect and model-dependent determinations of $\pi\pi$ phase shifts cannot be correct. This explains the absence of $I=0 \ 0^{++}(750)$

TABLE VIII. Results of the fits to two of four solutions of the S-wave intensity measured in $\pi^- p \to \pi^- \pi^+ n$ at 17.2 GeV/c using the χ^2 minimization method for amplitude analysis. The fits are made with Breit-Wigner parametrization (6.3) and (6.4) with the Pišút-Roos shape factor.

I_S Solution	m_σ (MeV)	Γ_σ (MeV)	B	N_S	$\chi^2/N_{\rm DF}$
Single Breit-Wigner fit					
(1,1)	760±8	269±29		2.00±0.13	0.414
(2,2)	786±21	408±90		2.24±0.16	1.140
Breit-Wigner fit with constant background					
(1,1)	761±8	227±68	0.12±0.19	1.84±0.28	0.394
(2,2)	780±13	187±77	0.63±0.31	1.51±0.31	0.864

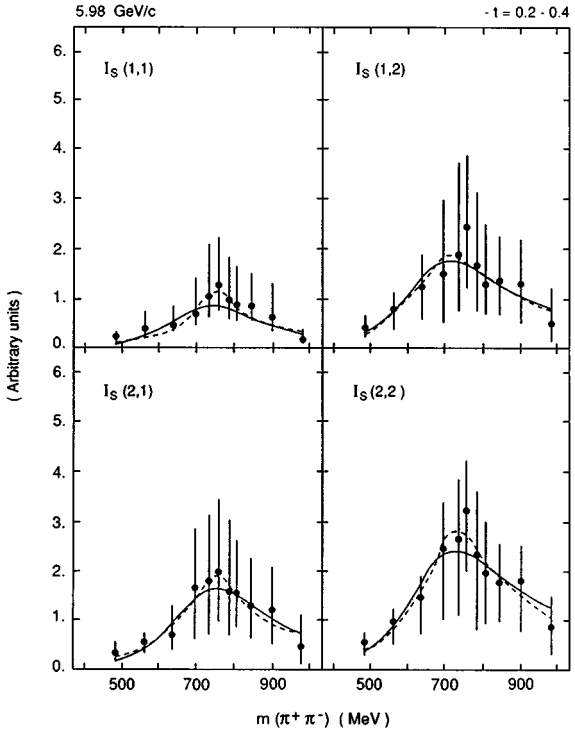

FIG. 9. Four solutions for the S-wave intensity I_S measured in $\pi^+ n_\uparrow \to \pi^+ \pi^- p$ at 5.98 GeV/c and $-t = 0.2-0.4$ (GeV/c)^2 using the Monte Carlo method for amplitude analysis (Ref. [25]). The solid and dashed curves are Breit-Wigner fits as in Fig. 7. The fitted parameters are given in Table IX.

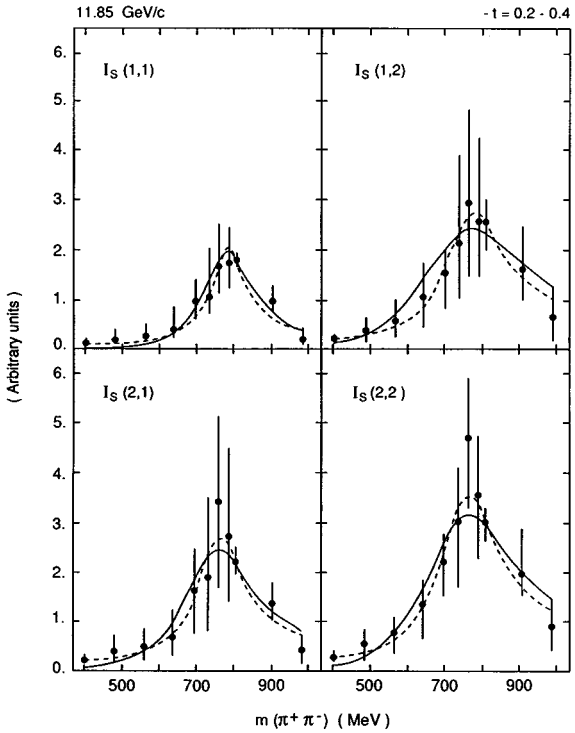

FIG. 10. Four solutions for the S-wave intensity I_S measured in $\pi^+ n_\uparrow \to \pi^+ \pi^- p$ at 11.85 GeV/c and $-t = 0.2-0.4$ (GeV/c)^2 using the Monte Carlo method for amplitude analysis (Ref. [25]). The solid and dashed curves are Breit-Wigner fits as in Fig. 7. The fitted parameters are given in Table X.

resonance in the δ_0^0 phase shift from these analyses.

We will now review the basic assumptions common to all determinations of $\pi\pi$ phase shifts [2,13–19]. *A priori*, there is no connection between the partial wave amplitudes in $\pi\pi \to \pi\pi$ scattering and the production amplitudes in $\pi N \to \pi^+\pi^- N$ reactions. We recall that in $\pi N \to \pi^+\pi^- N$ there are two S-wave production amplitudes $S(s,m,t)$ and $S(s,m,t)$ [or $S_0(s,m,t)$ and $S_1(s,m,t)$] while in $\pi\pi \to \pi\pi$ there is one S-wave amplitude (or phase shift δ_0^0) dependent only on the energy E. Also, in $\pi N \to \pi^+\pi^- N$ there are six P-wave production amplitudes L,L,U,U,N,N (or $L_n, U_n, N_n, n=0,1$) which depend on variables s,m,t while in $\pi\pi \to \pi\pi$ there is again one P-wave amplitude (or phase shift δ_1^1) dependent only on the energy E. To make the connection between the production amplitudes in $\pi N \to \pi^+\pi^- N$ and the partial-wave amplitudes in $\pi\pi \to \pi\pi$ the following assumptions of factorization and identification are postulated in all determinations of $\pi\pi$ phase shifts from unpolarized data on $\pi N \to \pi^+\pi^- N$.

The starting point is the dimeson helicity $\lambda = 0$ pion exchange amplitudes S_1 and L_1 in the t channel. It is assumed that the t and m dependence in these amplitudes factorizes

$$S_1(s,m,t) = N \frac{\sqrt{-t}}{t-\mu^2} F_0(t) \frac{m}{\sqrt{q}} f_0(m),$$

$$L_1(s,m,t) = N \frac{\sqrt{-t}}{t-\mu^2} F_1(t) \frac{m}{\sqrt{q}} f_1(m), \qquad (7.1)$$

where t is the momentum transfer at the nucleon vertex, m and q are the dipion mass and the π^- momentum in the $\pi^-\pi^+$ c.m. frame. The form factors $F_J(t)$ describe the t dependence and the functions $f_J(m)$, $J=0,1$, describe the mass dependence. N is a normalization constant. Furthermore, the functions $f_J(m)$ are assumed to be the partial-wave amplitudes in $\pi^-\pi^+ \to \pi^-\pi^+$ reaction at c.m. energy m:

$$f_0 = \frac{2}{3} f_0^{I=0} + \frac{1}{3} f_0^{J=2},$$

$$f_1 = f_1^{I=1}. \qquad (7.2)$$

The partial wave amplitudes f_J^I with definite isospin I are defined so that in the $\pi\pi$ elastic region

$$f_J^I = \sin\delta_J^I e^{i\delta_J^I}. \qquad (7.3)$$

The phase shifts δ_J^I are determined from the amplitudes S_1 and L_1 which are calculated from the data on $\pi^- p \to \pi^-\pi^+ n$ on an unpolarized target. However, the calculation of amplitudes S_1 and L_1 from the $\pi^- p \to \pi^-\pi^+ n$ data cannot be done without additional assumptions. There are simply more amplitudes than data. To proceed further all determinations of $\pi\pi$ phase shifts must assume that all A_1-exchange amplitudes vanish:

$$S_0 = L_0 = U_0 \equiv 0. \qquad (7.4)$$

TABLE IX. Results of the fits to the four solutions of the S-wave intensity measured in $\pi^+ n \to \pi^+ \pi^- p$ at 5.98 GeV/c using the Monte Carlo method for amplitude analysis. The fits are made with Breit-Wigner parametrization (6.3) and Eq. (6.4) with the Pišút-Roos shape factor.

I_S Solution	m_σ (MeV)	Γ_σ (MeV)	B	N_S	$\chi^2 N_{\rm DF}$
Single Breit-Wigner fit					
(1,1)	723±22	282±68		0.53±0.10	0.888
(1,2)	696±36	333±128		1.13±0.34	0.118
(2,1)	740±32	296±116		1.02±0.29	0.204
(2,2)	714±27	362±102		1.52±0.30	0.194
Breit-Wigner fit with constant background					
(1,1)	746±16	145±69	0.18±0.10	0.59±0.18	0.712
(1,2)	706±39	262±24	0.13±0.39	1.05±0.44	0.114
(2,1)	745±30	165±112	0.23±0.21	0.97±0.42	0.094
(2,2)	724±25	211±117	0.25±0.20	1.41±0.42	0.124

With the assumption (7.4), two solutions for the S-wave phase shift δ_0^0 are found [15,16]: the ''down'' solution which is nonresonating and the ''up'' solution which resonates at the mass around 770 MeV with a width of about 150 MeV. The resonating solution was rejected because it disagreed with the $\pi^0\pi^0$ mass spectrum from a low-statistics experiment [37] on $\pi^- p \to \pi^0\pi^0 n$ at 8 GeV/c.

There is no theoretical proof of factorization [Eq. (7.1)] and identification [Eq. (7.2)] of functions f_J with $\pi\pi$ partial-wave amplitudes. It is not obvious that the $\pi\pi$ phase shifts calculated from $\pi^- p \to \pi^- \pi^+ n$ data using the assumptions (7.1)–(7.3) would coincide with $\pi\pi$ phase shifts determined directly from real pion-pion scattering. Only such comparison could test the assumption (7.2).

The factorization (7.1) implies that the mass spectrum of amplitudes $|S_1|^2$ and $|L_1|^2$ is independent of t. This consequence of factorization can be tested in measurements of $\pi N \to \pi^+ \pi^- N$ on polarized targets. In Fig. 11 we show the t evolution of the mass dependence of the lower and upper bounds [10] on normalized moduli $|L|^2$, $|\overline{L}|^2$, $|U|^2$, and $|\overline{U}|^2$. The data at $t=-0.068$ (GeV/c)^2 are from $\pi^- p \to \pi^- \pi^+ n$ at 17.2 GeV/c, the rest are from $\pi^+ n \to \pi^+ \pi^- p$ at 5.98 GeV/c. Figure 11 shows a clear and pronounced dependence of mass spectra of amplitudes $|L|^2$ and $|\overline{L}|^2$ on momentum transfer t. In particular, there is a clear change of mass spectrum below $-t=0.25$ (GeV/c)^2, a region of t relevant to determinations of $\pi\pi$ phase shifts. While this change could be entirely due to A_1 exchange amplitude L_0, this cannot be guaranteed. The factorization assumption (7.1) thus cannot be taken for granted and further tests of this assumption are required in future high statistics measurements of $\pi N \to \pi^+ \pi^- N$ on polarized targets.

The assumption (7.4) of the absence of A_1-exchange amplitudes has several consequences that can be directly tested in measurements on polarized targets. From Eq. (2.13) we see that the absence of A_1-exchange amplitudes implies

$$|A| = |\overline{A}| \quad \text{for} \quad A = S, L, U. \tag{7.5}$$

The equality of moduli of amplitudes with the recoil nucleon transversity ''down'' and ''up'' is not observed experimentally. We can see in Figs. 1 and 2 that the S-wave amplitudes $|S|$ and $|\overline{S}|$ are clearly unequal at 17.2 GeV/c and $-t=0.005$–0.20 (GeV/c)^2. In Fig. 11 we see that the P-wave amplitudes $|L|$ and $|\overline{L}|$ are different in every t bin

TABLE X. Results of the fits to the four solutions of the S-wave intensity measured in $\pi^+ n \to \pi^+ \pi^- p$ at 11.85 GeV/c using Monte Carlo method for amplitude analysis. The fits are made with Breit-Wigner parametrization (6.3) and (6.4) with the Pišút-Roos shape factor.

I_S Solution	m_σ (MeV)	Γ_σ (MeV)	B	N_S	$\chi^2/N_{\rm DF}$
Single Breit-Wigner fit					
(1,1)	778± 10	158±21		1.19±0.12	2.158
(1,2)	749± 31	353±88		1.47±0.25	0.430
(2,1)	752± 20	237±52		1.50±0.27	0.844
(2,2)	749± 19	309±63		1.92±0.24	0.632
Breit-Wigner fit with constant background					
(1,1)	782±9	117±26	0.08±0.03	1.13±0.16	1.024
(1,2)	770±24	202±74	0.09±0.04	1.52±0.32	0.080
(2,1)	763±18	153±55	0.12±0.05	1.46±0.39	0.236
(2,2)	756±15	200±59	0.11±0.05	1.93±0.33	0.212

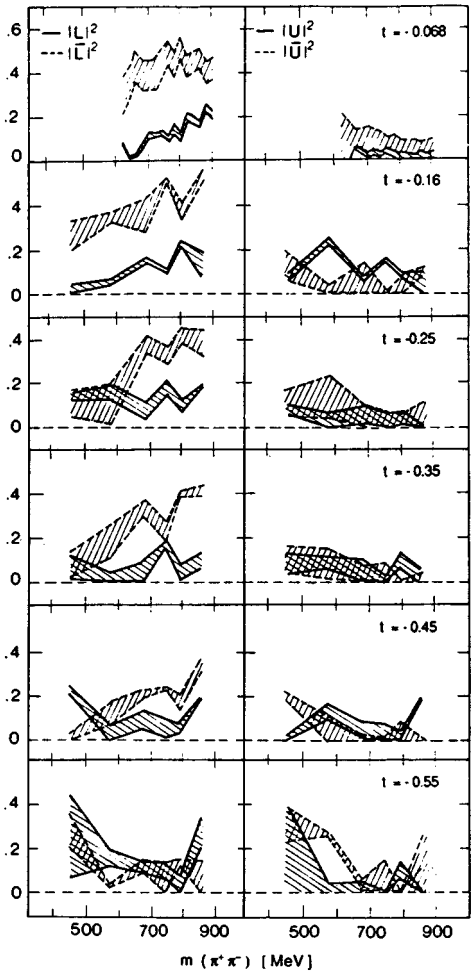

FIG. 11. The t evolution of the mass dependence of moduli squared of t-channel normalized transversity amplitudes $|L|^2$, $|\bar{L}|^2$, $|U|^2$, and $|\bar{U}|^2$ in $\pi^+ n_\uparrow \to \pi^+ \pi^- p$ at 5.98 GeV/c together with the results for $\pi^- p_\uparrow \to \pi^- \pi^+ n$ at 17.2 GeV/c and $t = 0.068$ (GeV/c)^2.

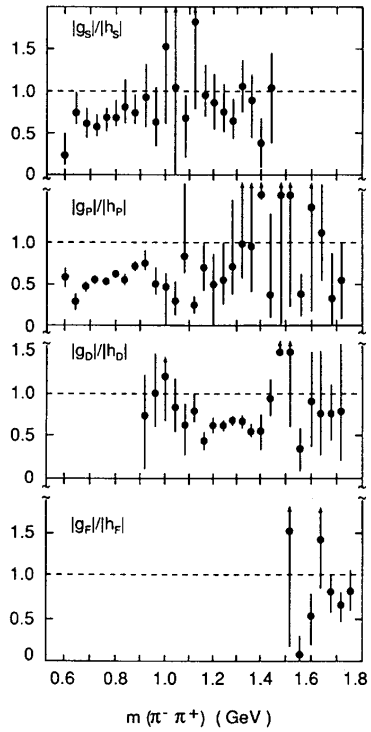

FIG. 12. The ratio of amplitudes with recoil nucleon transversity ''down'' and ''up'' with dimeson helicity $\lambda = 0$. The deviation from unity shows the strength of A_1-exchange amplitudes. Based on Fig. 6 of Ref. [5]. In our notation, $g_S = S$, $h_S = S$, $g_P = L$, $h_P = \bar{L}$.

from 0.005 to 0.60 (GeV/c)^2, and that the difference is largest at small t, the region of most importance to the determination of $\pi\pi$ phase shifts.

The A_1-exchange is large and nontrivial also above 900 MeV and in higher partial waves D and F. This finding of the CERN-Munich analysis [5] of $\pi^- p \to \pi^- \pi^+ n$ data on a polarized target in the mass range 600–1800 MeV is shown in Fig. 12. The figure shows the ratios of moduli of amplitudes with recoil nucleon transversity ''down'' and ''up'' for S-, P-, D-, and F-wave amplitudes with dimeson helicity $\lambda = 0$ which are directly relevant for the determination of the corresponding phase shifts. The deviations from 1 indicate the strength of the A_1 exchange. We can see in Fig. 12 that the A_1 exchange is important in all waves up to 1800 MeV at small $-t = 0.005$–0.20 (GeV/c)^2. The determinations of $\pi\pi$ phase shifts above 900 MeV also assumed the absence of A_1-exchange amplitudes. We must conclude that the determinations of $\pi\pi$ phase shifts from S wave to F wave in the mass region from 600 to 1800 MeV are not reliable. Theoretical calculations and analyses based on these phase shifts are therefore not reliable as well.

Below 1000 MeV, where the S and P wave dominate, the assumptions (7.4) lead to predictions for polarized SDM elements that can be directly compared with the data. The predictions of Eq. (7.4) are [25]

$$\rho^y_{ss} + \rho^y_{00} + 2\rho^y_{11} = -2(\rho^y_{00} - \rho^y_{11}) = +2\rho^y_{1-1}, \qquad (7.6)$$

$$\mathrm{Re}\rho^y_{10} = \mathrm{Re}\rho^y_{1s} = \mathrm{Re}\rho^y_{0s} \equiv 0. \qquad (7.7)$$

The data for polarized SDM elements clearly rule out these predictions as is shown in Figs. 13 and 14 for $\pi^- p \to \pi^- \pi^+ n$ at 17.2 GeV/c. We find that $\rho^y_{ss} + \rho^y_{00} + 2\rho^y_{11}$ and $-2(\rho^y_{00} - \rho^y_{11})$ have large magnitudes but opposite signs while $2\rho^y_{1-1}$ has a small magnitude. The interference terms $\mathrm{Re}\rho^y_{10}$, $\mathrm{Re}\rho^y_{1s}$, and $\mathrm{Re}\rho^y_{0s}$ are all dissimilar and have large nonzero values. On the basis of this evidence we again must conclude that the past determinations of $\pi\pi$ phase shifts from unpolarized data on $\pi N \to \pi^+ \pi^- N$ are questionable.

The assumption of the absence of A_1-exchange amplitudes means that the pion production in $\pi N \to \pi^+ \pi^- N$ reactions does not depend on nucleon spin. What the measurements of $\pi N \to \pi^+ \pi^- N$ on polarized targets found is that the pion production depends strongly on nucleon spin. The dynamics of the pion production is not as simple as has been assumed in the past determinations of $\pi\pi$ phase shifts. New determinations of $\pi\pi$ phase shifts are now required that do take into account the existence of A_1 exchange. Since the contributions of A_1-exchange amplitudes are large and nontrivial, the revisions of $\pi\pi$ phase shifts will be significant. The new revised S-wave phase shift δ^0_0 is then expected to

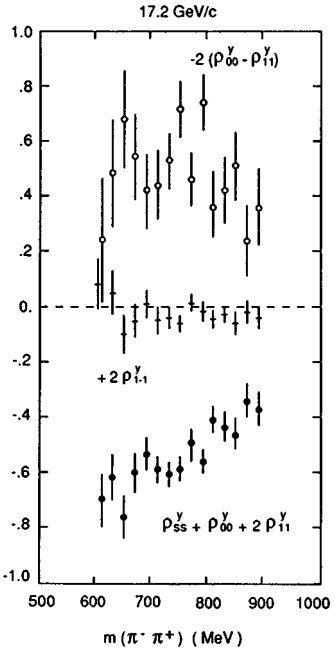

FIG. 13. Test of predictions $\rho^y_{ss}+\rho^y_{00}+2\rho^y_{11}=-2(\rho^y_{00}-\rho^y_{11})=+2\rho^y_{1-1}$ due to vanishing A_1 exchange in $\pi^- p_\uparrow \to \pi^-\pi^+ n$ at 17.2 GeV/c and $-t=0.005-0.2$ (GeV/c)^2.

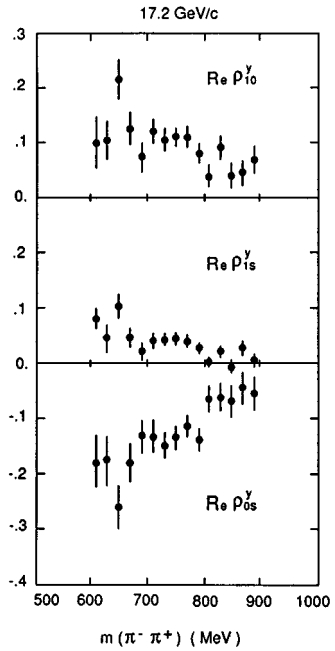

FIG. 14. Test of predictions $\mathrm{Re}\rho^y_{10}=\mathrm{Re}\rho^y_{1s}=\mathrm{Re}\rho^y_{0s}=0$ due to vanishing A_1 exchange in $\pi^- p_\uparrow \to \pi^-\pi^+ n$ at 17.2 GeV/c and $-t=0.005-0.2$ (GeV/c)^2.

show evidence for narrow scalar state $\sigma(750)$ in agreement with the measurements on polarized targets.

VIII. QUESTIONS CONCERNING EVIDENCE FOR NARROW $\sigma(750)$

A. Up-down ambiguity and analyticity constraints

Recently it has been claimed [36,38,39] that $\pi\pi$ phase shift δ^0_0 can be determined from the S-wave intensities I_S obtained in our amplitude analysis of $\pi^- p \to \pi^-\pi^+ n$ on a polarized target at 17.2 GeV/c, and that it would show the old up-down ambiguity of δ^0_0. Only the up solution indicates a narrow σ state and it is excluded because it is inconsistent with the Roy equations [40]. From this it was concluded that $\sigma(750)$ does not exist [38] or that the evidence must be treated with reservation [36,39].

To answer this objection we first recall from Eq. (2.15) that

$$I_S=(|S_0|^2+|S_1|^2)\Sigma. \tag{8.1}$$

Here the amplitude S_1 is connected to δ^0_0 through Eqs. (7.1) and (7.3), and S_0 is the unknown A_1-exchange amplitude. It is obvious from this expression that the determination of δ^0_0 from data on I_S depends on the model used for A_1 exchange amplitude S_0. The data on the polarized target require large A_1-exchange amplitudes. At present the A_1-exchange amplitudes are not known. We must therefore conclude that the phase shift δ^0_0 cannot be determined from the data on S-wave intensity I_S at present.

Nevertheless, the data on I_S do tell us something very important about the solutions for δ^0_0. There are four solutions for I_S: $I_S(1,1),\ldots,I_S(2,2)$. Consequently there will be a fourfold ambiguity in δ^0_0 for any given model of A_1-exchange amplitude S_0. However, as can be seen in Fig. 7, the four solutions for I_S are all very similar quantitatively. Consequently the four solutions for δ^0_0 are expected to be very close to each other and similar. This contrasts with the large differences between the old up and down solutions. Figure 15 shows the S-wave intensity normalized to 1 at the maximum for down (curve A) and up (curve B) solutions from the typical analysis of Estabrooks and co-workers [15,16]. The large differences between the up and down solutions contrast sharply with the small differences shown between S-wave intensities $I_S(1,1)$ and $I_S(2,2)$ in Fig. 15. On the basis of the similar behavior of all solutions for I_S we do not anticipate the emergence of the old up-down ambiguity problem in δ^0_0. It is even possible that the small differences between the four solutions for I_S can be explained entirely as a small ambiguity in A_1-exchange amplitude S_0 leading to a unique determination of δ^0_0 from the data on polarized target.

The above discussion applies also to the determination of P-wave phase shift δ^1_1 from $I_L=(|L_0|^2+|L_1|^2)\Sigma$. The amplitude L_1 is connected to δ^1_1 by Eqs. (7.1) and (7.3) while L_0 is another unknown A_1-exchange amplitude. The four solutions for I_L are again very close so we expect similar solutions for δ^1_1.

Assuming a model for A_1-exchange amplitudes S_0 and L_0, the obtained phase shifts δ^0_0 and δ^1_1 can be tested for consistency with dispersion relations [40] (Roy equations). If an inconsistency is found it means that we have to modify our model for A_1-exchange amplitudes S_0 and L_0, and try again. It is important to realize that Roy equations do not test the validity of the experimentally measured amplitudes $|S|^2$, $|\overline{S}|^2$, $|L|^2$, $|\overline{L}|^2$, or intensities I_S and I_L. The Roy equations are constraints only on $\pi\pi$ phase shifts which follow from the analyticity properties of partial wave amplitudes in $\pi\pi\to\pi\pi$ scattering. However, the requirement of a consis-

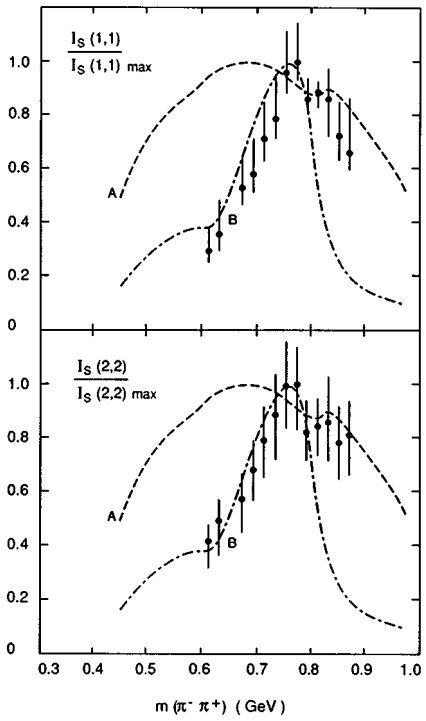

FIG. 15. S-wave intensity normalized to 1 at maximum value. The data correspond to solutions $I_S(1,1)$ and $I_S(2,2)$ at 17.2 (GeV/c) from Ref. [25]. The smooth curves are predictions of phase shift analysis for $\pi^+\pi^-\to\pi^+\pi^-$ from Ref. [15]. The dashed curve is the accepted solution down, the dot-dashed curve is the rejected solution up.

tency of phase shifts with the Roy equations can be used to constrain the possible models of A_1-exchange amplitudes.

We conclude that the experimental evidence for the narrow state $\sigma(750)$ is not in contradiction with analyticity and dispersion relations for $\pi\pi$ partial waves. The existence of A_1 exchange and narrow $\sigma(750)$ are experimental findings from measurements on polarized targets independent of the Roy equations. These experimental facts cannot be refuted by comparisons with standard phase shifts because these were obtained using an invalid assumption of absence of A_1 exchange.

B. The absence of $\sigma(750)$ in $\gamma\gamma\to\pi^+\pi^-$ and central production $pp\to pp\pi^+\pi^-$

Morgan and Pennington suggested discounting the evidence for existence of narrow $\sigma(750)$ in $\pi N\to\pi^+\pi^- N$ because this state has not been observed in the $\gamma\gamma\to\pi^+\pi^-$ reaction [38] and in central production [38,41] $pp\to pp\pi^+\pi^-$. However, there are good reasons why one would not expect to observe narrow $\sigma(750)$ in these processes.

In the next section we shall argue that the narrow $\sigma(750)$ is the lowest mass scalar gluonium $0^{++}(gg)$. The principal support for this proposal is precisely the fact that the $\sigma(750)$ state is not observed in the $\gamma\gamma\to\pi^+\pi^-$ reaction. Since gluons do not couple directly to the photons, we expect $\sigma(750)$ not to appear in the reaction $\gamma\gamma\to\pi^+\pi^-$ if it is pure gluonium or if it has only a small $q\bar{q}$ component.

The reaction $pp\to pp\pi^+\pi^-$ was measured [42] at the CERN Intersecting Storage Rings (ISR) in a search for scalar gluonium. The structures reported in the moments $H(11)$ and $H(31)$ near $m(\pi^+\pi^-)\approx 750$ MeV are consistent with $\sigma(750)$ and $\rho^0(770)$ interference.

Assuming parity conservation there are five S-wave amplitudes and 15 P-wave amplitudes in this reaction. The $\sigma(750)$ state may contribute only to some S-wave amplitudes and not to the others, as it does in $\pi^- p\to\pi^-\pi^+ n$ with amplitudes $|S|^2\Sigma$ and $|S|^2\Sigma$. As we see in Fig. 7, the S-wave intensity $I_S(2,2)$ does not immediately suggest the existence of a narrow $\sigma(750)$. With five S-wave amplitudes in $pp\to pp\pi^+\pi^-$ it is very likely that $\sigma(750)$ stays hidden. We can observe $\sigma(750)$ in $\pi^- p\to\pi^-\pi^+ n$ and $\pi^+ n\to\pi^+\pi^- p$ reactions only when these production processes are measured on polarized targets, and the S- and P-wave amplitudes can be separated in a model-independent way. For the same reasons we may see $\sigma(750)$ in central production $pp\to pp\pi^+\pi^-$ only when measurements with polarized initial protons are made and the resonating S-wave amplitudes can be isolated. The ISR experiment does not separate the S- and P-wave amplitudes, and thus is not conclusive.

C. Comparison with other results for the σ state

The DM2 Collaboration measured [43] $\pi^+\pi^-$ mass distribution in $J/\psi\to\omega\pi^+\pi^-$ decays and observed a quite broad low mass resonance [see Fig. 13(a) of Ref. [43]]. Interpreted as an $I=0$ 0^{++} σ state, a single Breit-Wigner fit gives $m_\sigma=(414\pm 20)$ MeV, $\Gamma_\sigma=(494\pm 58)$ MeV. There is no indication for such a state in our data on S-wave intensity I_S in $\pi^+ n\to\pi^+\pi^- p$ at 5.98 and 11.85 GeV/c (see Figs. 9 and 10 above). The reasons for the discrepancy are not clear at the present.

Several recent theoretical analyses [44–46] claimed existence of a σ meson with a mass around 1000 MeV and a broad width of 460–880 MeV. These analyses use as an input the S-wave phase shift δ_0^0 and thus neglect the A_1 exchange and other spin effects observed in pion production (see, e.g., Eq. (5) in Ref. [44]). It is possible that when these analyses include in their fits A_1 exchange that they will find a narrow σ in agreement with the CERN data on polarized targets.

IX. CONSTITUENT STRUCTURE OF THE $\sigma(750)$ RESONANCE

In the usual quark model meson resonances are $q\bar{q}$ states. The mass of $\sigma(750)$ is too low for it to be a $q\bar{q}$ state. The mass M of the $q\bar{q}$ state increases with its angular momentum L as $M=M_0(2n+L)$, where n is the degree of radial excitation. The lowest mass scalar mesons are $^3P_0$ states with masses expected to be around 1000 MeV or higher.

It was suggested that $0^{++}(700)$ could be a four-quark $q\bar{q}q\bar{q}$ state in the MIT bag model [47]. However, more detailed studies of $q\bar{q}q\bar{q}$ systems conclude that pure multiquark hadrons do not exist [48,49] with $\pi^+\pi^-$ decay [50]. We can also exclude the possibility that $\sigma(750)$ is a hybrid state $q\bar{q}g$. The lowest mass hybrid state must be a 0^{-+} or 1^{-+} state. Calculations based on bag models, QCD sum rules,

lattice QCD, and a string model all estimate [51] the masses of $0^{++}(q\bar{q}g)$ states to be above 1500 MeV.

Ellis and Lanik discussed the couplings of scalar gluonium σ on the basis of the low-energy theorems of broken chiral symmetry and scale invariance, implemented using a phenomenological Lagrangian [52]. They obtained for $\sigma\to\pi^+\pi^-$ decay the following partial width:

$$\Gamma(\sigma\to\pi^+\pi^-)=\frac{(m_\sigma)^5}{48\pi G_0}, \tag{9.1}$$

where $G_0\equiv\langle 0|(\alpha_s/\pi)F_{\mu\nu}F^{\mu\nu}|0\rangle$ is the gluon-condensate term [53] parametrizing the nonperturbative effects in QCD. The numerical values were estimated by the ITEP group [53] to be $G_0\approx 0.012$ (GeV)^4 or up to $G_0\approx 0.030$ (GeV)^4 in later calculations [54,55]. Several recent estimates of G_0 all agree on the values around $G_0\approx 0.020$ (GeV)^4 [56–58]. It is very interesting to note, that when we take $G_0=0.015$ (GeV)^4 the Ellis-Lanik theorem (9.1) predicts partial width $\Gamma(\sigma\to\pi^+\pi^-)=107$ MeV for the mass $m_\sigma=753$ MeV. This result is in perfect agreement with Eq. (4.21), where $\Gamma_\sigma=108\pm 53$ MeV. When we use for m_σ the value 768 MeV obtained in interference fits with $f_0(980)$ then the Ellis-Lanik theorem predicts a partial width $\Gamma(\sigma\to\pi^+\pi^-)=118$ MeV, again in perfect agreement with Eq. (5.6), where $\Gamma_\sigma=115\pm 38$ MeV. However, Γ_σ is the full width of $\sigma(750)$ so these results on $\Gamma(\sigma\to\pi^+\pi^-)$ represent upper limits. When we use $G_0=0.020$ (GeV)^4, which is the average of the latest values for G_0 [56–58], we get for the partial width $\Gamma(\sigma\to\pi^-\pi^+)=0.75\Gamma_\sigma$ with a very reasonable branching fraction of 75% for the $\pi^-\pi^+$ channel. From this agreement with the Ellis-Lanik theorem we can conclude that the $\sigma(750)$ is best understood as the lowest mass gluonium state $0^{++}(gg)$.

The gluonium interpretation of $\sigma(750)$ gathers further support from the lack of observation of $\sigma(750)$ in the reactions $\gamma\gamma\to\pi^+\pi^-$ and $\gamma\gamma\to\pi^0\pi^0$. Since gluons do not couple directly to photons we expect $\sigma(750)$ not to appear in reactions $\gamma\gamma\to\pi\pi$ if it is a pure gluonium state or if it contains only a small $q\bar{q}$ component. This conclusion is supported by the PLUTO and DELCO data [59,60]. However, the more recent DM1/2 data [61,62] show an excess over the Born term expectation that is attributed to the formation of a broad scalar resonance with a two-photon width of (10 ± 6) MeV. This would suggest some $q\bar{q}$ component in the $\sigma(750)$ state. The most recent results [63] are on $\gamma\gamma\to\pi^0\pi^0$ which show no evidence for a scalar state near 750 MeV.

Lattice QCD calculations by several groups [64–67] initially concluded that the gluonium ground state $0^{++}(gg)$ has a mass near the ρ^0 meson: 740 ± 40 MeV. The most recent lattice QCD calculations predict a much higher mass of the lowest scalar gluonium: the UKQCD group [68] predicts 1550 ± 50 MeV while the IBM group [69,70] predicts 1740 ± 70 MeV. However, it is important to remember that these calculations are for quenched QCD so there is no coupling of the primitive gluonium to quarks. The coupling of gluonium to two pseudoscalars may have a significant effect on the gluonium mass and width [41].

We conclude that while the gluonium interpretation of the $\sigma(750)$ state is in agreement with low-energy theorems of broken chiral symmetry and scale invariance, it is at variance with the most recent lattice QCD calculations. It is necessary to study this discrepancy and understand its origins and implications.

Finally we note that the anomalous energy dependence of pp and np elastic polarizations and the departure from the mirror symmetry in πN elastic polarizations at intermediate energies require a low-lying Regge trajectory [71,72] corresponding to $\sigma(750)$. These anomalous structures in the polarization data may have been the first evidence for a gluonium exchange in two-body reactions.

X. SUMMARY

The measurements of reactions $\pi^- p_\uparrow\to\pi^-\pi^+ n$ at 17.2 GeV/c and $\pi^+ n_\uparrow\to\pi^+\pi^- p$ at 5.98 and 11.85 GeV/c on a polarized target provide model-independent and solution-independent evidence for a narrow scalar state $\sigma(750)$. The amplitude analyses of $\pi^- p_\uparrow\to\pi^-\pi^+ n$ at small t using the χ^2 minimization method [4] and the Monte Carlo method [25] yield very similar results for moduli of transversity amplitudes and cosines of their relative phases. In particular they agree that the transversity ''up'' S-wave amplitude $|S|^2\Sigma$ resonantes near 750 MeV while the transversity ''down'' amplitude $|S|^2\Sigma$ is nonresonating and constitutes a large background in the spin-averaged S-wave intensity $I_S=(|S|^2+|S|^2)\Sigma$. For this reason it is preferable to determine resonance parameters of $\sigma(750)$ directly from the measured mass distribution of $|S|^2\Sigma$.

We have performed several types of Breit-Wigner fits to $|S|^2\Sigma$. We have shown that the Pišút-Roos resonance shape formula and phenomenological shape formula give similar results. Single Breit-Wigner fits yield a width of $\sigma(750)$ in the range 192–256 MeV. We have studied the effect of background in three approaches: the incoherent background, the constant coherent background, and the t-averaged constant coherent background. The last method yields the best fit with the lowest $\chi^2/N_{\rm DF}$. The solution and method average for the σ mass and width from this best fit are

$$m_\sigma=753\pm 19\ \ \text{MeV},\quad \Gamma_\sigma=108\pm 53\ \ \text{MeV}. \tag{10.1}$$

We also performed the conventional fits to spin-averaged S-wave intensity I_S. We found again that the inclusion of background (incoherent in this case) reduces the fitted value of the σ width and improves $\chi^2/N_{\rm DF}$. Nevertheless, the direct fits to $|S|^2\Sigma$ are preferable at 17.2 GeV. Due to lower statistics at 5.98 and 11.85 GeV/c, we must use results for I_S to obtain σ resonance parameters. All four solutions resonate at these larger momentum transfers but yield a broader σ width: $\Gamma_\sigma=195\pm 81$ MeV at 5.98 GeV/c and $\Gamma_\sigma=166\pm 54$ MeV at 11.85 GeV/c. We conclude that the best overall estimate of the mass and width of $\sigma(750)$ are the values in Eq. (10.1) from the best fit to $|S|^2\Sigma$ (Table IV).

We have also examined the interference of $\sigma(750)$ with $f_0(980)$ and found that it has only a small effect on the mass and width of $\sigma(750)$. A fit to amplitude $|S|^2\Sigma$ in the mass range above 1120 MeV shows evidence for a scalar state with average mass 1280 ± 12 MeV and width 192 ± 26 MeV.

The conventional S-wave phase shifts δ_0^0 show no evidence for the narrow $\sigma(750)$ state. It must be reiterated, that the past determinations of $\pi\pi$ phase shifts from unpolarized data on $\pi^- p \to \pi^- \pi^+ n$ assumed the absence of A_1-exchange amplitudes. This assumption is invalidated by measurements of $\pi^- p \to \pi^- \pi^+ n$, $\pi^+ n \to \pi^+ \pi^- p$, and $K^+ n \to K^+ \pi^- p$ on polarized targets which find large and nontrivial A_1-exchange contributions. New determinations of $\pi\pi$ phase shifts are required that do take into account the existence of A_1 exchange. Since A_1-exchange contributions are large, the revisions of $\pi\pi$ phase shifts will be significant and should provide evidence for a narrow $\sigma(750)$ state in agreement with the CERN data on polarized targets.

The mass of $\sigma(750)$ is too low for it to be a $q\bar{q}$ state. We proposed to identify $\sigma(750)$ with the lowest mass scalar gluonium $0^{++}(gg)$. This proposal is supported by the perfect agreement with the Ellis-Lanik theorem (9.1) relating the decay width of scalar gluonium $\Gamma(\sigma \to \pi^+ \pi^-)$ to its mass m_σ. Another experimental support for the gluonium interpretation of $\sigma(750)$ is its absence in $\gamma\gamma \to \pi^+ \pi^-$ reaction. However, the low mass of $\sigma(750)$ is at variance with the more recent calculations of lattice QCD which predict masses of scalar gluonium above 1500 MeV.

Experiments with polarized targets have opened a whole new approach to experimental hadron spectroscopy by making accessible the study of hadron production on the level of production spin amplitudes. We may expect that a new generation of high statistics measurements of various pion production processes [12,73,74] at different values of t [10] will further develop hadron spectroscopy and our understanding of hadron dynamics.

ACKNOWLEDGMENTS

I wish to thank V. P. Kanavets, P. Lichard, M. D. Scadron, J. Stern, and especially N. A. Törnqvist for their interest, and their stimulating correspondence. This work was supported by Fonds pour la Formation de Chercheurs et l'Aide à la Recherche (FCAR), Ministère de l'Education du Québec, Canada.

[1] G. Lutz and K. Rybicki, Max Planck Institute, Munich, Internal Report No. MPI-PAE/Exp. E1.75, 1978 (unpublished).
[2] G. Grayer *et al.*, Nucl. Phys. **B75**, 189 (1974).
[3] J. G. H. de Groot, Ph.D. thesis, University of Amsterdam, 1978.
[4] H. Becker *et al.*, Nucl. Phys. **B150**, 301 (1979).
[5] H. Becker *et al.*, Nucl. Phys. **B151**, 46 (1979).
[6] V. Chabaud *et al.*, Nucl. Phys. **B223**, 1 (1983).
[7] K. Rybicki and I. Sakrejda, Z. Phys. C **28**, 65 (1985).
[8] A. de Lesquen *et al.*, Phys. Rev. D **32**, 21 (1985).
[9] A. de Lesquen *et al.*, Phys. Rev. D **39**, 21 (1989).
[10] M. Svec, A. de Lesquen, and L. van Rossum, Phys. Rev. D **42**, 934 (1990).
[11] M. Svec, A. de Lesquen, and L. van Rossum, Phys. Rev. D **45**, 55 (1992).
[12] M. Svec, A. de Lesquen, and L. van Rossum, Phys. Rev. D **45**, 1518 (1992).
[13] S. D. Protopopescu *et al.*, Phys. Rev. D **7**, 1279 (1973).
[14] B. Hyams *et al.*, Nucl. Phys. **B64**, 134 (1973).
[15] P. Estabrooks and A. D. Martin, in *$\pi\pi$ Scattering-1973*, Proceedings of the International Conference on $\pi\pi$ Scattering, Tallahassee, 1973, edited by D. K. Williams and V. Hagopian, AIP Conf. Proc. No. 13 (AIP, New York, 1973), p. 37.
[16] P. Estabrooks and A. D. Martin, Nucl. Phys. **B79**, 301 (1974).
[17] P. Estabrooks and A. D. Martin, Nucl. Phys. **B95**, 322 (1975).
[18] K. L. Au, D. Morgan, and M. R. Pennington, Phys. Rev. D **35**, 1633 (1987).
[19] B. S. Zou and D. V. Bugg, Phys. Rev. D **48**, R3948 (1993).
[20] M. Anselmino, A. Efremov, and E. Leader, Phys. Rep. **261**, 1 (1995).
[21] J. T. Donohue and Y. Leroyer, Nucl. Phys. **B158**, 123 (1979).
[22] See S-wave intensity I_S in Fig. 2 of Ref. [5].
[23] See S-wave intensity I_S in Fig. 10 of Ref. [11].
[24] M. Svec, A. de Lesquen, and L. van Rossum, Phys. Rev. D **46**, 949 (1992).
[25] M. Svec, Phys. Rev. D **53**, 2343 (1996).
[26] J. Pišút and M. Roos, Nucl. Phys. **B6**, 325 (1968).
[27] M. Aguilar-Benítez and J. A. Rubio, ''Hadronic Resonances Part II: Experimental Analyses,'' Grupo Inter-universitario de Fisica Teorica de Atlas Energias Report No. GIFT4/75, Vol. 2, 1975 (unpublished).
[28] H. Pilkuhn, *The Interactions of Hadrons* (North-Holland, Amsterdam, 1967).
[29] C. D. Lac *et al.*, J. Phys. (France) **51**, 2689 (1990).
[30] P. W. Johnson, R. C. Miller, and G. M. Thomas, Phys. Rev. D **7**, 1895 (1977).
[31] H. Palka, Institute of Nuclear Physics, Cracow, Internal Report No. 1230/PH, 1983, Appendix D (unpublished).
[32] F. James, in *Techniques and Concepts of High Energy Physics II*, edited by Thomas Ferbel (Plenum, New York, 1983), p. 196.
[33] I. Silin, computer code FUMILI, Long Write-up D510, CERN Computer Centre Program Library, revised 1985.
[34] J. M. Blatt and V. F. Weiskopf, *Theoretical Nuclear Physics* (Wiley, New York, 1952).
[35] N. A. Törnqvist (private correspondence).
[36] Particle Data Group, R. M. Barnett *et al.*, Phys. Rev. D **54**, 355 (1996).
[37] W. D. Apel *et al.*, Phys. Lett. **41B**, 542 (1972).
[38] D. Morgan, in *Hadron 93*, Como, Italy, 1993 [Nuovo Cimento A **107**, 1883 (1994)].
[39] Particle Data Group, L. Montanet *et al.*, Phys. Rev. D **50**, 1173 (1994), p. 1478.
[40] M. R. Pennington and S. D. Protopopescu, Phys. Rev. D **7**, 2591 (1973).
[41] M. R. Pennington, in *Hadron 95*, Manchester 1995, edited by M. K. Birke, G. Lafferty, and J. McGovern (World Scientific, Singapore, 1996), p. 3.
[42] T. Akesson *et al.*, Phys. Lett. **133B**, 263 (1983).

[43] DM2 Collaboration, J. Augustin *et al.*, Nucl. Phys. **B320**, 1 (1989).
[44] N. N. Achasov and G. N. Shestakov, Phys. Rev. D **49**, 5779 (1994).
[45] V. V. Anisovich *et al.*, Phys. Lett. B **355**, 363 (1995).
[46] N. A. Törnqvist and M. Roos, Phys. Rev. Lett. **76**, 1575 (1996).
[47] R. J. Jaffe, Phys. Rev. D **15**, 267 (1977).
[48] R. P. Bickerstaff and B. H. McKellar, Z. Phys. C **16**, 171 (1982).
[49] J. Weinstein and N. Isgur, Phys. Rev. D **27**, 588 (1983).
[50] B. A. Liu and K. F. Liu, Phys. Rev. D **30**, 6139 (1984).
[51] F. E. Close, Nucl. Phys. **A416**, 55c (1984).
[52] J. Ellis and J. Lanik, Phys. Lett. **150B**, 289 (1985).
[53] M. S. Shifman, A. I. Vainshtein, and V. I. Zakharov, Nucl. Phys. **B147**, 385 (1975); **B147**, 448 (1979).
[54] J. S. Bell and R. A. Bertlmann, Nucl. Phys. **B177**, 218 (1981); **B187**, 285 (1981).
[55] A. Bradley, C. S. Largensiepen, and G. Shaw, Phys. Lett. **102B**, 359 (1981).
[56] S. Narison, Phys. Lett. B **387**, 162 (1996).
[57] S. Bertolini, in Proceedings of the Workshop on *K* Physics, Orsay, France, 1996, Report No. hep-ph/9607312 (unpublished).
[58] M. Fabbrichesi, in Proceedings of the Workshop on *K* Physics, Orsay, France, 1996, Report No. hep-ph/9607348 (unpublished).
[59] Ch. Berger *et al.*, Z. Phys. C **26**, 199 (1984).
[60] H. Aihara *et al.*, Phys. Rev. Lett. **57**, 404 (1986).
[61] A. Coureau *et al.*, Nucl. Phys. **B271**, 1 (1986).
[62] Z. Ajaltouni *et al.*, Phys. Lett. B **194**, 573 (1987); **197**, 565(E) (1987).
[63] H. Marsiske *et al.*, Phys. Rev. D **41**, 3324 (1990).
[64] K. Ishikawa *et al.*, Phys. Lett. **116B**, 429 (1982).
[65] K. Ishikawa *et al.*, Z. Phys. C **21**, 327 (1983); **21**, 167 (1983).
[66] B. Berg and A. Billoire, Nucl. Phys. **B221**, 109 (1983).
[67] W. H. Hamber and M. Urs Meiller, Phys. Rev. D **29**, 928 (1984).
[68] G. Bali *et al.*, Phys. Lett. B **309**, 378 (1993).
[69] F. Butler *et al.*, Phys. Rev. Lett. **70**, 2849 (1993).
[70] M. Chen *et al.* in *Lattice '93*, Proceedings of the International Symposium, Dallas, Texas, edited by T. Draper *et al.* [Nucl. Phys. B (Proc. Suppl.) **34**, 357 (1994)].
[71] J. W. Dash and H. Navelet, Phys. Rev. D **13**, 1940 (1976).
[72] G. Girardi and H. Navelet, Phys. Rev. D **14**, 280 (1976).
[73] M. Svec, Phys. Rev. D **55**, 4355 (1997).
[74] M. Svec, ''Amplitude analysis of reactions $\pi^- p \to \eta\pi^- p$ and $\pi^- p \to \eta\pi^0 n$ measured on polarized target and the exotic 1^{-+} meson,'' McGill University, Report No. hep-ph/9608475, 1996 (unpublished).